Satellite Observations of Stratospheric Hydrogen Fluoride and Comparisons with SLIMCAT Calculations

by

Jeremy J. Harrison[1,2], Martyn P. Chipperfield[3,4], Christopher D. Boone[5], Sandip S. Dhomse[3,4], Peter F. Bernath[6], Lucien Froidevaux[7], John Anderson[8], and James Russell III[8]

[1]*Department of Physics and Astronomy, University of Leicester, Leicester LE1 7RH, United Kingdom.*

[2]*National Centre for Earth Observation, University of Leicester, Leicester LE1 7RH, United Kingdom.*

[3]*Institute for Climate and Atmospheric Science, School of Earth and Environment, University of Leeds, Leeds LS2 9JT, United Kingdom.*

[4]*National Centre for Earth Observation, School of Earth and Environment, University of Leeds, Leeds LS2 9JT, United Kingdom.*

[5]*Department of Chemistry, University of Waterloo, Waterloo, Ontario N2L 3G1, Canada.*

[6]*Department of Chemistry and Biochemistry, Old Dominion University, Norfolk, Virginia 23529, United States of America.*

[7]*Jet Propulsion Laboratory, Pasadena, California 91109, United States of America.*

[8]*Department of Atmospheric and Planetary Sciences, Hampton University, Hampton, Virginia 23668, United States of America.*

Number of pages   = 30
Number of tables   = 5
Number of figures = 11

Address for correspondence:
            Dr. Jeremy J. Harrison
            National Centre for Earth Observation
            Department of Physics and Astronomy
            University of Leicester
            University Road
            Leicester LE1 7RH
            United Kingdom
Tel: (44)-116-2231943

e-mail: jh592@leicester.ac.uk

39   **Abstract**

40   The vast majority of emissions of fluorine-containing molecules are anthropogenic

41   in nature, e.g. chlorofluorocarbons (CFCs), hydrochlorofluorocarbons (HCFCs), and

42   hydrofluorocarbons (HFCs). Many of these fluorine-containing species deplete stratospheric

43   ozone, and are regulated by the Montreal Protocol. Once in the atmosphere they slowly

44   degrade, ultimately leading to the formation of HF, the dominant reservoir of stratospheric

45   fluorine due to its extreme stability. Monitoring the growth of stratospheric HF is therefore

46   an important marker for the success of the Montreal Protocol.

47   We report the comparison of global distributions and trends of HF measured in the

48   Earth's atmosphere by the satellite remote-sensing instruments ACE-FTS (Atmospheric

49   Chemistry Experiment Fourier Transform Spectrometer), which has been recording

50   atmospheric spectra since 2004, and HALOE (HALogen Occultation Experiment), which

51   recorded atmospheric spectra between 1991 and 2005, with the output of SLIMCAT, a state-

52   of-the-art three-dimensional chemical transport model. In general the agreement between

53   observation and model is good, although the ACE-FTS measurements are biased high by

54   ~10% relative to HALOE. The observed global HF trends reveal a substantial slowing down

55   in the rate of increase of HF since the 1990s: 4.97 ± 0.12 %/year (1991-1997; HALOE), 1.12

56   ± 0.08 %/year (1998-2005; HALOE), and 0.52 ± 0.03 %/year (2004-2012; ACE-FTS). In

57   comparison, SLIMCAT calculates trends of 4.01 %/year, 1.10 %/year, and 0.48 %/year,

58   respectively, for the same periods; the agreement is very good for all but the earlier of the

59   two HALOE periods. Furthermore, the observations reveal variations in the HF trends with

60   latitude and altitude, for example between 2004 and 2012 HF actually decreased in the

61   southern hemisphere below ~35 km. An additional SLIMCAT simulation with repeating

62   meteorology for the year 2000 produces much cleaner trends in HF with minimal variations

63   with latitude and altitude. Therefore, the variations with latitude and altitude in the observed

64   HF trends are due to variability in stratospheric dynamics on the timescale of a few years.

65   Overall, the agreement between observation and model points towards the ongoing success of

66   the Montreal Protocol and the usefulness of HF as a metric for stratospheric fluorine.

67

1. Introduction

The accumulation of fluorine in the Earth's atmosphere has resulted from anthropogenic emissions of organic molecules such as chlorofluorocarbons (CFCs), hydrochlorofluorocarbons (HCFCs), and hydrofluorocarbons (HFCs). The long atmospheric lifetimes of such molecules allow them to reach the stratosphere, where they break down and liberate fluorine in various inorganic forms. The most abundant of the emitted organic source molecules are CFC-12 (CCl_2F_2), CFC-11 (CCl_3F), CFC-113 (CCl_2FCClF_2), which are all now banned under the Montreal Protocol because they deplete stratospheric ozone, and HCFC-22 ($CHClF_2$), the most abundant HCFC and a transitional substitute under the Protocol. Although long-lived, these molecules do degrade in the atmosphere at high altitudes, ultimately to the long-lived stratospheric reservoir molecule hydrogen fluoride, HF; the chemistry schemes are presented below. Monitoring HF as part of the atmospheric fluorine family is important in closing the fluorine budget, particularly as anthropogenic emissions of fluorine species, many of which are ozone-depleting and all of which are greenhouse gases, have varied substantially over time. Certainly, monitoring the growth of stratospheric HF, which has slowed in recent years, is an important marker for the success of the Montreal Protocol (in addition to monitoring stratospheric HCl).

For the three most abundant fluorine source gases, CFC-12, CFC-11, and HCFC-22, atmospheric degradation proceeds with the breaking of a C-Cl (CFC-12 and CFC-11) or C-H (HCFC-22) bond (Ricaud and Lefevre, 2006),

$$CCl_2F_2 + hv \rightarrow CClF_2 + Cl$$
$$CCl_3F + hv \rightarrow CCl_2F + Cl$$
$$CHClF_2 + OH \rightarrow CClF_2 + H_2O. \qquad (R1)$$
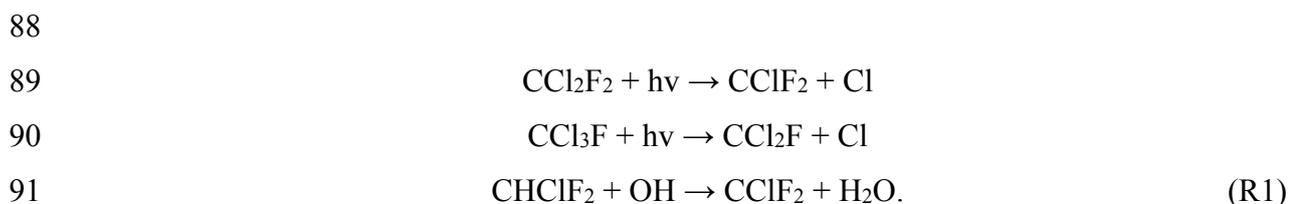
Depending on their structure, the intermediates produced in R1 react further,

$$CClF_2 + O_2 + M \rightarrow CClF_2O_2 + M$$
$$CClF_2O_2 + NO \rightarrow CClF_2O + NO_2$$
$$CClF_2O + O_2 \rightarrow COF_2 + ClO_2, \qquad (R2)$$

$$CCl_2F + O_2 + M \rightarrow CCl_2FO_2 + M$$
$$CCl_2FO_2 + NO \rightarrow CCl_2FO + NO_2$$
$$CCl_2FO + O_2 \rightarrow COClF + ClO_2. \qquad (R3)$$

3
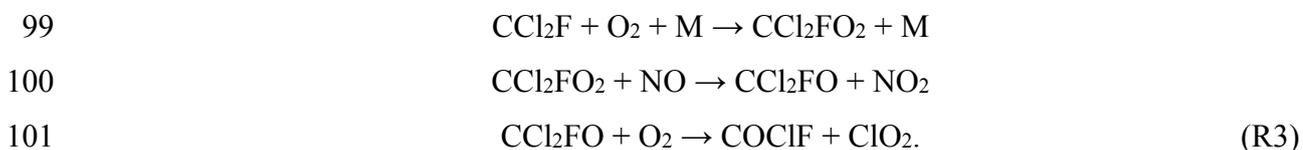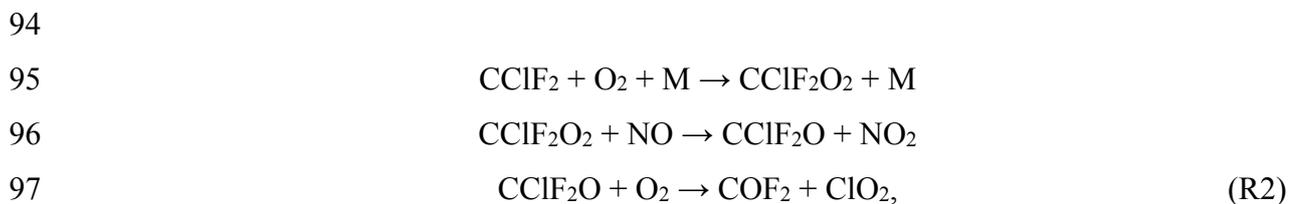
102

103   For CFC-113, and minor sources such as HFCs (e.g. HFC-134a, HFC-152a), the reaction
104   scheme is similar.

105   In Equations R2 and R3, carbonyl chloride fluoride (COClF) and carbonyl fluoride
106   (COF_2), are important 'inorganic' reservoirs (the common terminology in atmospheric
107   science differs from that in chemistry) of fluorine in the stratosphere, with lifetimes of 1.6
108   (Fu et al., 2009) and 3.8 (Harrison et al., 2014) years, respectively; COF_2 is more abundant
109   than COClF. The trends in these inorganic reservoirs over time are directly related to the
110   trends of the individual source gases. The decrease in the amounts of atmospheric CFC-11
111   and CFC-113, the principal sources of carbonyl chloride fluoride, has led to a decreasing
112   trend in this reservoir (Brown et al., 2011), whereas carbonyl fluoride is still slowly
113   increasing over time due to the increase in HCFC-22, which more than compensates for the
114   decrease in the CFC-12 and CFC-113 source gases (Brown et al., 2011; Harrison et al.,
115   2014).

116   COClF and COF_2 volume mixing ratios (VMRs) slowly increase with altitude
117   through the lower stratosphere until they reach their respective maxima, at ~25 – 30 km for
118   COClF (Fu et al., 2009) and ~30 – 40 km for COF_2 (Harrison et al., 2014). Above these
119   altitudes photolysis becomes more efficient, leading to the formation of fluorine atoms,

120

$$COF_2 + h\nu \rightarrow FCO + F$$
$$COClF + h\nu \rightarrow FCO + Cl$$
$$FCO + O_2 + M \rightarrow FC(O)O_2 + M$$
$$FC(O)O_2 + NO \rightarrow FCO_2 + NO_2$$
$$FCO_2 + h\nu \rightarrow F + CO_2. \tag{R4}$$
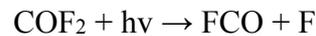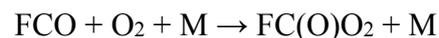
121
122
123
124
125

126

127   The liberated fluorine atoms then react with methane, water or molecular hydrogen, to form
128   the inorganic product hydrogen fluoride, HF. At the top of the stratosphere most of the
129   fluorine is present as HF (Brown et al., 2014), the dominant reservoir of stratospheric
130   fluorine due to its extreme stability. Note that due to this stability, F is not important for
131   catalytic stratospheric ozone loss. HF is removed from the stratosphere by slow transport to,
132   and rainout in, the troposphere, or by upward transport to the mesosphere, where it is
133   destroyed by photolysis (Duchatelet et al., 2010). Overall the amount of HF in the
134   atmosphere is increasing (e.g. Brown et al., 2014).

135   The first detection of HF in the Earth's stratosphere, based on solar spectra recorded

136   from balloon and on the ground at Jungfraujoch, was made by Zander et al. (1977).

137   Measurements continue to be made at Jungfraujoch using a ground-based Fourier transform

138   spectrometer (FTS), (e.g. Duchatelet et al., 2010). There have also been measurements of HF

139   taken, for example, by the Atmospheric Trace MOlecule Spectrometry Experiment

140   (ATMOS) instrument which flew four times on NASA Space Shuttles between 1985 and

141   1994 (Irion et al., 2002) and the MkIV interferometer, a balloon-borne solar occultation FTS

142   (Velazco et al., 2011). Measurements taken by satellite-borne instruments, however, allow

143   HF to be observed with global coverage, and seasonal and latitudinal variability to be

144   investigated fully. The first global atmospheric distributions of HF were provided by the

145   HALogen Occultation Experiment (HALOE) instrument, onboard the Upper Atmosphere

146   Research Satellite (UARS), which recorded atmospheric spectra between 1991 and 2005.

147   More recently, the Atmospheric Chemistry Experiment (ACE)-FTS, onboard the SCISAT

148   satellite, has been recording atmospheric spectra since 2004, carrying the mantle of HF

149   measurements into the second decade of the twenty-first century. In fact, the ACE-FTS is the

150   only satellite instrument currently taking measurements of HF.

151   This paper follows on from our recent work on the global distributions and trends of

152   COF_2, the most important 'temporary' stratospheric fluorine reservoir that directly leads to

153   the formation of HF. The aim of the present work is to understand the HF global distribution

154   and trends derived from satellite observations taken by the HALOE and ACE-FTS

155   instruments. To do this, we use the SLIMCAT model, a state-of-the-art three-dimensional

156   (3D) chemical transport model (CTM), one of the few to include stratospheric fluorine

157   chemistry. Additionally, we compare tracer-tracer correlations between some of the major

158   HF 'sources' for SLIMCAT and satellite observations as a further test of the model

159   chemistry.

160

161   **2. Hydrogen fluoride datasets**

162   **2.1. ACE-FTS**

163   The ACE-FTS instrument, which covers the spectral region 750 to 4400 cm^{-1} with a

164   maximum optical path difference (MOPD) of 25 cm and a resolution of 0.02 cm^{-1} (using the

165   definition of 0.5/MOPD throughout), uses the sun as a source of infrared radiation to record

166   limb transmission through the Earth's atmosphere during sunrise and sunset ('solar

167   occultation'). Transmittance spectra are obtained by ratioing against exo-atmospheric 'high

168   sun' spectra measured each orbit. These spectra, with high signal-to-noise ratios, are

169   recorded through long atmospheric limb paths (~300 km effective length), thus providing a

170   low detection threshold for trace species. ACE has an excellent vertical resolution of about

171   3-4 km and can measure up to 30 occultations per day, with each occultation sampling the

172   atmosphere from 150 km down to the cloud tops (or 5 km in the absence of clouds). The

173   locations of ACE occultations are dictated by the low Earth circular orbit of the SCISAT

174   satellite and the relative position of the sun. Over the course of a year, the ACE-FTS records

175   atmospheric spectra over a large portion of the globe (Bernath et al., 2005), from which it is

176   possible to extract profiles of many fluorine-containing species, including CCl_3F (CFC-11),

177   CCl_2F_2 (CFC-12), $CHClF_2$ (HCFC-22), CCl_2FCClF_2 (CFC-113), CH_3CCl_2F (HCFC-141b),

178   CH_3CClF_2 (HCFC-142b), CH_2FCF_3 (HFC-134a), CHF_3 (HFC-23), CF_4, COF_2, COClF, HF

179   and SF_6.

180   The atmospheric pressure and temperature profiles, the tangent heights of the

181   measurements, and the hydrogen fluoride VMRs were taken from version 3.0 (January 2004

182   until September 2010) and v3.5 (from October 2010) processing of the ACE-FTS data. Note

183   that the retrieval scheme is identical for both the v3.0 and v3.5 datasets, the difference being

184   in the meteorological data used as input for the pressure and temperature retrievals (the

185   lowest ACE-FTS levels use these data directly). Due to an error in these inputs, v3.0 data

186   should only be used for measurements taken until the end of September 2010, while v3.5 is

187   valid for all ACE-FTS measurements. Details of the retrieval scheme for versions 3.0/3.5

188   processing have been explained elsewhere (e.g., Boone et al., 2013; Harrison et al., 2014).

189   Briefly, vertical profiles of trace gases (along with temperature and pressure) are derived

190   from the recorded transmittance spectra via an iterative Levenberg-Marquardt nonlinear

191   least-squares global fit to the selected spectral region(s) for all measurements within the

192   altitude range of interest. The microwindow set and associated altitude ranges for the HF

193   retrieval are listed in Table 1. The VMRs for molecules with absorption features in the

194   microwindow set (see Table 2) were adjusted simultaneously with the HF amount. All

195   spectroscopic line parameters were taken from the HITRAN 2004 database (Rothman et al.,

196   2005), with HF parameters apparently unchanged since HITRAN 1992. The microwindow

197   set covers eight spectroscopic lines (P_1, P_2, P_3, P_4, R_0, R_1, R_2, R_3) from the fundamental (1-0)

198   band of HF. The HF retrieval extends from a lower altitude of 12 km up to altitudes

199   corresponding to an atmospheric density of 9.0×10^{15} molecules cm^{-3}, in practice ~50-55 km,

200   thus providing a variation in upper altitude with both latitude and season (see Table 1). The

201   HF spectral signal in ACE-FTS spectra recorded above the upper altitude retrieval limit is

202   generally below the noise level, so it is not possible to retrieve VMRs directly at these

203   altitudes. Instead, the VMR profile above the highest analysed ACE measurement is

204   calculated by scaling the 'initial' VMR profile, taken from ATMOS measurements (Irion et

205   al., 2002), over these altitudes; the scaling factor is determined during the least-squares

206   fitting.

207

208   **2.2. HALOE**

209   Like the ACE-FTS, the HALOE instrument (Russell et al., 1993) used the principle

210   of solar occultation to sound the middle atmosphere at sunset and sunrise (relative to the

211   instrument). HALOE used broadband and gas-filter radiometry, with channels covering

212   selected portions of the spectrum between 2.45 and 10.04 μm, to determine the mixing ratios

213   of molecules related to the chemistry of stratospheric ozone and its destruction by CFCs. In

214   particular, HALOE provided measurements of O_3, HCl, HF, CH_4, H_2O, NO, NO_2, aerosol

215   extinction, and temperature versus pressure, over an altitude range of ~15 to 60 – 130 km

216   depending on channel (HF, HCl, CH_4 and NO were measured using gas filter radiometry).

217   As with the ACE-FTS, the locations of HALOE occultations and hence the extent of its

218   global coverage were dictated by its orbit and the relative position of the sun. HALOE, with

219   an orbit inclination of 57º compared with 74º for the ACE-FTS, had a more even latitudinal

220   coverage and provided more data over tropical regions, for example, than the ACE-FTS

221   which takes most of its measurements at high latitude.

222   The atmospheric pressure, temperature, tangent heights, and hydrogen fluoride

223   VMRs were taken from version 19 processing of the HALOE data, which are available from

224   October 1991 to November 2005. The retrieval scheme incorporates a simple 'onion

225   peeling' approach stabilised at the top and bottom of the profile with a scalar optimal

226   estimation formulation developed by Connor and Rodgers (1989). For the HF channel, the

227   spectral bandpass 5% relative response points are 4025 cm^{-1} and 4135 cm^{-1}. The HF spectral

228   line parameters were taken from the HITRAN 1992 database (Rothman et al., 1992). The

229   instantaneous vertical field-of-view in the limb is ~1.6 km. Detailed validation studies for

230   HALOE HF measurements were published by Russell et al. (1996). Note that for internal

231   consistency with previous work on the fluorine budget (Brown et al., 2014) and COF_2

232   (Harrison et al., 2014), the vertical pressure grid has been interpolated onto the standard 1-km

233   grid used by the ACE-FTS.

234

235   **2.3. GOZCARDS**

236   The ACE-FTS, HALOE and SLIMCAT model time series are also compared with
237   those of the GOZCARDS (Global OZone Chemistry And Related Datasets for the
238   Stratosphere) HF data product in Section 5.   GOZCARDS provides a global long-term
239   stratospheric Earth System Data Record (ESDR) for stratospheric ozone and related chemical
240   species, including HF.   The HF data record was not ready in time to be included in the
241   original dataset provided for public usage (temperature, O_3, H_2O, HCl, N_2O, and HNO_3); we
242   are presenting the HF data for the first time here. Froidevaux et al. (2015) have described the
243   GOZCARDS data creation methodology and some stratospheric characteristics concerning
244   the latter five species.   The constituent datasets are time series of monthly zonal means
245   versus latitude (in 10º latitude bins) taken from existing satellite datasets.   In particular, the
246   GOZCARDS HF data product is derived by merging the v19 HALOE (1991 – 2005) and
247   v2.2 ACE-FTS (2004 – 2010) datasets, with the relative bias between source datasets
248   removed by averaging them over the overlap period 2004 – 2005 and adjusting the series
249   accordingly; note that such a process does not account for any systematic biases in the
250   original datasets.   All GOZCARDS datasets are provided on a vertical pressure grid.   Again,
251   to be consistent with previous ACE work, this vertical pressure grid has been interpolated
252   onto the standard 1-km grid used by the ACE-FTS.   Note that as this GOZCARDS dataset
253   uses v2.2 ACE-FTS data, the time series terminates in September 2010.
254

255   **3. Retrieval errors**

256   **3.1. Infrared spectroscopy of hydrogen fluoride**

257   One of the major sources of systematic error for any retrieved atmospheric profile
258   arises from uncertainties in the laboratory spectroscopic data.   A discussion of spectroscopic
259   errors is therefore appropriate.   The ACE-FTS retrieval makes use of HF line parameters first
260   made available as part of the HITRAN 1992 database (and remaining unchanged until the
261   HITRAN 2012 release), with partition data taken from the Total Internal Partition Sums
262   (TIPS) subroutine included in the HITRAN compilation.   HITRAN simply provides error
263   codes for line parameters in the form of uncertainty ranges, but with no information as to
264   how the parameters are correlated.   For the HF line parameters used in this work, the errors
265   correspond to $0.0001 – 0.001$ cm^{-1} for the line wavenumber, ν, $2 – 5$ % for the line intensity,
266   S, and $1 – 2$ % for the air-broadened half-width, γ_{air}.   Errors are unreported for γ_{self} (self-
267   broadened half-width), n_{air} (temperature-dependence exponent for γ_{air}), and δ_{air} (air pressure-
268   induced line shift).   Recently, and after v3.0 processing of the ACE data was complete,
269   HITRAN 2012 became available; it includes a complete re-evaluation of HF spectroscopy.

270 The associated publication (Rothman et al., 2013) also explains that all the air-broadening

271 parameters, γ_{air}, for the fundamental band of HF were fitted with the Galatry profile, not the

272 Voigt profile, which is the lineshape of choice for the HITRAN database. Additionally, the

273 Dicke narrowing parameters in the original analysis were simply neglected. For the purposes

274 of this work, we assume a retrieval error of at most ~4 % arising from uncertainties in HF

275 line parameters.

276

277 **3.2. ACE-FTS**

278   The ACE v2.2 HF data product, which uses a slightly different microwindow set

279 from v3.0/v3.5 as well as an earlier version of the PT retrieval, has previously been validated,

280 for example, against measurements taken by HALOE and the MkIV interferometer (Mahieu

281 et al., 2008). It was found that ACE-FTS v2.2 HF measurements are biased high compared

282 to HALOE, with mean differences around 5–20% between 15 and 49 km. Comparison of

283 ACE-FTS v2.2 HF with MkIV data is generally good, with relative differences above 19 km

284 within ±10%. There have been no detailed comparisons in the literature between ACE-FTS

285 v2.2 and v3.0 HF datasets, although Duchatelet et al. (2010) suggest that ACE-FTS v3.0 HF

286 VMRs have decreased by close to 5% relative to v2.2. However, a re-evaluation of filtered

287 v2.2 and v3.0/v3.5 HF data carried out as part of this work indicates good agreement within ±

288 5 %, with no significant overall bias between the two datasets.

289   The 1σ statistical fitting errors for a single ACE profile are typically ~5 % over most

290 of the altitude range. These errors are random in nature and largely determined by the

291 measurement noise of the ACE-FTS. Averaged profiles tend to be dominated by systematic

292 errors, with random errors reduced by a factor of $1/\sqrt{N}$, where N is the number of profiles

293 averaged. Spectroscopic sources of systematic error predominantly arise from the HF

294 HITRAN linelist (~4 %; see Section 3.1), with minor contributions from interfering species

295 that absorb in the microwindow regions; we assume that these contributions are small, at

296 most 1 %, due to the lack of systematic features in the spectral residuals (Harrison et al.,

297 2014). Additional systematic errors arise from uncertainties in temperature, pressure, tangent

298 altitude (i.e. pointing) and instrumental line shape (ILS); these were estimated by running the

299 ACE-FTS retrieval for a subset of occultations, with each quantity (b_j) perturbed in turn by

300 its assumed 1σ uncertainty (Δb_j). The fractional retrieval error, μ_j, is defined as

301

$$302 \qquad \mu_j = \left| \frac{VMR(b_j + \Delta b_j) - VMR(b_j)}{VMR(b_j)} \right|. \qquad (3)$$

303

304 Note that pressure, temperature and tangent height are not strictly independent quantities for

305 ACE-FTS retrievals; tangent heights are determined from hydrostatic equilibrium, and so

306 these quantities are strongly correlated. Therefore, only two of these three quantities are

307 altered: temperature is adjusted by 2 K and tangent height by 150 m (Harrison et al., 2014).

308 ILS uncertainty is determined by adjusting the field of view by 5 % (Harrison et al., 2014).

309 A subset of 81 occultations measured between 65º and 70ºN in July 2010 was selected for

310 this analysis. The fractional value estimates of the systematic uncertainties, and their

311 symbols, are given in Table 3. Assuming uncorrelated quantities, the overall systematic error

312 in the HF retrieval can be calculated as

313

$$314 \qquad \mu_{systematic}^2 = \mu_{spec}^2 + \mu_{int}^2 + \mu_T^2 + \mu_z^2 + \mu_{ILS}^2. \qquad (4)$$

315

316 The total systematic error contribution to the ACE-FTS HF retrieval is estimated to be ~10 %

317 over the altitude range of the retrieval.

318 As discussed in Section 3.1, HF VMRs are not directly retrieved for ACE

319 measurements taken at tangent heights above the upper altitude limits listed in Table 1. In

320 the ACE-FTS HF retrieval, the calculated spectrum is generated from the sum of

321 contributions from the tangent layer up to 150 km. For the highest analysed measurement,

322 the retrieved VMR in the tangent layer is generated from the piecewise quadratic

323 interpolation scheme (Boone et al., 2013), while the VMR in every layer above that is

324 determined from scaling the 'initial' VMR profile, with the scaling factor determined during

325 the retrieval by forcing the calculated spectrum to match as best as possible the measured

326 spectrum for the highest analysed measurement. Since the 'initial' profile is fixed to a

327 constant VMR between 50 and 100 km altitude, and since this portion of the profile is scaled

328 based on the VMR of the highest analysed ACE measurement, this will likely introduce

329 systematic errors into the highest altitudes of the retrieved profile. However, since the

330 scaling factor errors are dominated by the 1σ statistical fitting errors of the highest analysed

331 ACE measurement, it is anticipated that the systematic errors at the top of the profiles are

332 reduced when they are averaged to create zonal means.

333

3.3. HALOE

As discussed in Section 3.2, HALOE v19 HF has been validated against ACE-FTS v2.2, with the ACE measurements biased high by around 5–20% between 15 and 49 km (Mahieu et al., 2008). Furthermore, HF data from the MkIV interferometer for three flights (2003 – 2005) agree well with ACE-FTS, with relative differences above 19 km within ±10%, suggesting that there is a low bias in HALOE. Detailed HALOE HF error estimates and validation studies have previously been conducted by Russell et al. (1996). The estimated errors range from ~27% at 100 hPa to 15% at 1 hPa. Actual mean differences between HALOE and balloon data from a series of nine FTS under-flights, five operating in the far-IR and four MkIV comparisons in the near-IR, collectively ranged from more than 17% below 70 hPa where the mixing ratio is very low to <7% above that level, with no positive or negative bias implied. These HALOE data were produced using an early algorithm version, but results have proven to be very stable for later versions.

4. TOMCAT/SLIMCAT 3D Chemical Transport Model

SLIMCAT, an off-line 3D CTM, calculates the abundances of a number of stratospheric trace gases from prescribed source-gas surface boundary conditions and a detailed treatment of stratospheric chemistry, including the major species in the O_x, NO_y, HO_x, F_y, Cl_y and Br_y chemical families (e.g. Chipperfield, 1999; Feng et al., 2007). The model uses winds from meteorological analyses to specify winds and temperatures. This approach gives a realistic stratospheric circulation (Chipperfield, 2006; Monge-Sanz et al., 2007). In the version used here the troposphere is assumed to be well-mixed.

For this study SLIMCAT was integrated from 1977 to 2013 at a horizontal resolution of 5.6º × 5.6º and 32 levels from the surface to 60 km. The model uses a σ-p vertical coordinate (Chipperfield, 2006) and was forced by European Centre for Medium-Range Weather Forecasts (ECMWF) reanalyses (ERA-Interim from 1979 onwards). The VMRs of source gases at the surface level were specified using datasets prepared for the WMO/UNEP (2011) ozone assessment. These global mean surface values define the long-term tropospheric source gas trends in the model. Similarly, specification of the surface VMRs of degradation products acts as a sink for these species. The model initialisation used the estimated halocarbon loading for 1977, taken from the WMO/UNEP scenarios.

The SLIMCAT run makes use of the same chemistry scheme that was previously used for our work on COF_2 (Harrison et al., 2014), however in the present version the photolysis scheme has been updated to use latitudinally and monthly varying ozone profile

11

368 shapes in the photolysis look-up table. All source and degradation products related to
369 fluorine chemistry are listed in Table 4. COF_2 contributions arise from the degradation of
370 CFC-12, CFC-113, CFC-114, CFC-115, HCFC-22, HCFC-142b, HFC-23, HFC-134a, HFC-
371 152a, Halon 1211, and Halon 1301, with COClF production arising from the degradation of
372 CFC-11, CFC-113, and HCFC-141b (CH_3CCl_2F). Some HF is assumed to form directly
373 from the source gases (see Table 4), however this is almost negligible in practical terms (~3
374 % in 2010, mainly arising from HFC-134a). The relative amounts of HF formed (in 2010)
375 via COClF and COF_2 are 30 and 67 %, respectively.

376 The SLIMCAT calculations reveal that at altitudes above the maximum COClF and
377 COF_2 VMRs, there is net loss of these at all latitudes. The primary loss of COF_2 and COClF
378 in the stratosphere occurs via photolysis, with an additional secondary loss mechanism
379 through reaction with $O(^1D)$; SLIMCAT calculates relative contributions of 90 % and 10 %,
380 respectively, for COF_2 (Harrison et al., 2014) and 98 % and 2 % for COClF. The SLIMCAT
381 outputs enable an estimation of the atmospheric lifetimes of COF_2 and COClF by dividing
382 the total modelled atmospheric burden of each species by the total calculated atmospheric
383 loss rate. The total calculated mean atmospheric lifetimes are 3.9 years for COF_2, revised
384 upwards from the calculated value of 3.8 years presented by Harrison et al. (2014), and 1.7
385 years for COClF.

386

5. Comparison between ACE-FTS/HALOE/SLIMCAT datasets

388 The ACE-FTS HF data were binned into five latitude bands by month; VMRs
389 outside six median absolute deviations (MAD) of the median VMR for each bin and altitude
390 were removed from the analysis. Once filtered to remove significant outliers, the data were
391 used to create monthly zonal means at each altitude within 5° latitude bins. In Figure 1 these
392 have been plotted next to SLIMCAT zonal means for the months September 2009 to August
393 2010, thereby revealing the seasonal variation in the HF distribution over this period. Note
394 that these dates have been chosen to match those used in the previous work on carbonyl
395 fluoride (see Figure 11 of Harrison et al., 2014). The HF profiles generally show an increase
396 in VMR with altitude, with the rate of this increase varying with latitude and time of year.
397 Note that ACE-FTS observations do not cover all latitude bins over a single month (see
398 Section 2.1), and that latitude bins containing fewer occultations are noisier in appearance.
399 Despite these caveats, Figure 1 reveals a good agreement between the ACE-FTS observations
400 and the model which reproduces very well the significant seasonal variation. For example,
401 note in particular the agreement for regions of low HF VMR (< 1000 ppt) at ~30 – 40 km

402   over the southern tropics in February 2010 and the northern tropics in August 2010; at
403   southern mid- to high-latitudes in December 2009, and March and August 2010; and at
404   northern mid- to high-latitudes in February and March 2010.

405   Plots of ACE-FTS and HALOE HF observations side-by-side with SLIMCAT HF
406   calculations for September 2004 to August 2005 are shown in Figure 2. As for Figure 1, the
407   agreement between observations and model is generally good and the significant seasonal
408   variation is well reproduced. Note that, as for the ACE-FTS, HALOE data do not cover all
409   latitude bins in a given month, although HALOE does take more measurements at lower
410   latitudes. One noticeable difference revealed in Figure 2 is the relative low bias of HALOE
411   measurements compared with ACE-FTS and SLIMCAT; this is most notable at the top of the
412   altitude range. Using the period of overlap between ACE and HALOE, we can estimate that
413   ACE v3.0 is biased high by about 10% relative to HALOE. Biases between observations and
414   SLIMCAT will be more fully addressed in Section 6.

415   The overall atmospheric distribution of HF is determined by a complicated
416   combination of its production and transport, which depends on the production and lifetimes
417   of its 'sources' COF_2 and COClF. Figure 3 shows the observed and modelled COF_2 and
418   COClF zonal means for October 2009, and February and August 2010. Due to the upwelling
419   of relatively organic-fluorine-rich air in the tropical regions, the largest VMRs of COF_2 and
420   COClF are found over the tropics (Harrison et al., 2014; Fu et al., 2009), where solar
421   insolation is highest due to the small solar zenith angle, at altitudes of ~30 – 40 and ~25 – 30
422   km. For COF_2 the model agrees well with the ACE observations in terms of magnitude and
423   spatial distribution. For COClF the modelled distribution agrees with ACE but the peak
424   VMR is overestimated. Analysis of the SLIMCAT simulation shows that there is net loss of
425   COF_2 and COClF at altitudes above those of the maximum VMRs, at all locations. There is
426   therefore a correlation between the stratospheric regions of low HF VMR (< 1000 ppt) above
427   ~20 km at the poles and ~25 km at the equator and those of peak COF_2 and COClF VMRs.

428   Figure 1 reveals an asymmetry in the seasonal HF distribution between the two
429   hemispheres. This is attributable to asymmetries in the distributions of the 'sources' COF_2 /
430   COClF and their precursors, due to differences in the meridional Brewer-Dobson circulation,
431   and to the stronger descent of air associated with the winter polar vortex in the southern
432   hemisphere; for example, compare the enhanced ACE-FTS HF VMRs near the southern pole
433   in August 2010 with those near the northern pole in February 2010 at ~25 km. An additional
434   source of asymmetry in the COF_2 distribution, which directly influences the HF distribution,
435   arises from the temperature-dependent loss reaction of the COF_2-precursor $CHClF_2$ (HCFC-

436   22) with OH, leading to a secondary COF_2 maximum at southern hemisphere high-latitudes

437   in the summer mid-stratosphere (~10 K warmer than the corresponding location in the

438   northern hemisphere) (Harrison et al., 2014); for example, compare the ACE-FTS HF

439   southern hemisphere VMRs at ~30-35 km in January 2010 with those in the northern

440   hemisphere in July 2010.

441   In addition to side-by-side comparisons of model and observation, the chemistry

442   scheme in SLIMCAT can be tested by comparing (chemically related) tracer-tracer

443   correlations for model and observation; only ACE measurements of fluorine-containing HF

444   'precursors' are available for this purpose. It is widely known that all long-lived species in

445   the stratosphere have compact correlations, even if there is no chemical link between them.

446   As explained by Plumb and Ko (1992), two tracers with lifetimes longer than quasi-

447   horizontal mixing time scales should be in 'slope equilibrium' and produce a compact

448   correlation. Species with lifetimes longer than vertical transport time scales will also be in

449   'gradient equilibrium' and the compact correlation will be linear. Furthermore, relative

450   lower-stratospheric lifetimes of long-lived species (with stratospheric sinks via photolysis or

451   reaction with $O(^1D)$) under gradient equilibrium can be derived from the linear slope of the

452   tracer-tracer correlation (Chipperfield et al., 2014).

453   In the lower stratosphere COF_2 and $COClF$ can be regarded as long-lived tracers

454   (local lifetimes of many years). Therefore, their tracer isopleths should follow the typical

455   tropopause-following contours of any long-lived tracer. In this sense, COF_2 and $COClF$ are

456   analogous to NO_y which is produced from N_2O. Figure 4 contains correlation plots between

457   COF_2 and its major source, CFC-12, over the two latitude bands 65-70ºS and 65-70ºN for

458   two months each over the period September 2009 – August 2010. Comparisons are made at

459   high latitudes, where ACE-FTS observations are more plentiful, and for individual months to

460   ensure that time trends in the source gas VMRs are minimised. The figure reveals that COF_2

461   is indeed long-lived enough to show a good anti-correlation with CFC-12 in the lower

462   stratosphere. Furthermore, agreement between the model and observations is good although

463   there are a few discrepancies around the region of maximum COF_2 VMR; these are due to

464   issues surrounding the scaled a priori used in the retrieval for this altitude region of the

465   profile where the spectral signal has dropped to within the noise level (refer to Harrison et al.

466   (2014) for more details).

467   Figure 5 contains correlation plots between $COClF$ and its major source, CFC-11,

468   for the same conditions as in Figure 4. Unlike for COF_2 / CFC-12, the agreement between

469   model and ACE-FTS is particularly poor and the model overestimates the peak observed

14

470   values of COClF; this can also be observed in Figure 3. There are several possible reasons

471   for this. Firstly, as the modelled VMRs are ~50 % higher than the ACE-FTS VMRs, the

472   modelled COClF lifetime might be too long, i.e. the model underestimates the COClF loss

473   processes. This would result in the calculated HF VMRs being slightly lower than they

474   should be, probably by less than a percent, but certainly by less than the uncertainty of the

475   ACE-FTS measurements. An additional SLIMCAT calculation with the COClF lifetime

476   lowered by a third does improve the agreement with observations. Secondly, the COClF

477   sources might be overestimated, however SLIMCAT calculations for CFC-11 reveal good

478   agreement with ACE-FTS observations, generally within 10% (Brown et al., 2011).

479   Additionally, the chemistry could be more complicated with additional destruction routes

480   missing from the model. Lastly, there could be a problem with the ACE-FTS retrieval itself.

481   The COClF linelist used in the ACE-FTS retrieval was taken from the ATMOS database and

482   is described in the literature as 'very crude' (Perrin et al., 2011). At the time v3.0 data were

483   first released, this was the best linelist available, however a new and improved linelist has

484   subsequently been generated (Perrin et al., 2011), in which the band intensities are taken

485   from quantum-mechanical calculations. ACE-FTS COClF retrievals for a handful of

486   occultations have been carried out using the new linelist, however there is no improvement in

487   the disagreement with SLIMCAT.

488   It is expected that the sum of all fluorine source gas VMRs (not including those

489   which have very long lifetimes compared with the period of observations, e.g. CF_4 and SF_6)

490   is anti-correlated with total F_y VMR (HF + $2COF_2$ + COClF) in a conservative way (i.e. the

491   total adds up to a constant). As the ACE-FTS does not measure every source gas, and some

492   minor species have known biases (Brown et al., 2011), we only compare total F_y against the

493   sum of the major source gases, taken as CFC-11, CFC-12, and HCFC-22. The good

494   agreement between plots for SLIMCAT and ACE-FTS (see Figure 6) confirms that the

495   discrepancy in modelled and retrieved COClF VMRs has a minimal effect on the overall

496   agreement between model and observation for HF.

497

498   **6. Trends**

499   Since HF has no chemical sink, with only minor losses arising from rainout in the

500   troposphere and photolysis in the mesosphere, and since the atmosphere contains many long-

501   lived fluorine source gases, the overall HF atmospheric abundance has been increasing for

502   many years and is expected to increase in the foreseeable future. In this section trends in

503   ACE-FTS, HALOE, GOZCARDS and SLIMCAT time series are quantified as a function of

504   altitude and latitude. A number of previous studies have quantified trends; for example, a

505   linear trend of 8.5 ± 1.0%/year (1977 to 1986) (Zander et al., 1987) and 0.48 ± 0.25%/year

506   (2000 to 2009) (Kohlhepp et al., 2012) in total columns measured at Jungfraujoch (46.5ºN

507   latitude, 8.0ºE longitude), and 0.74 ± 0.2 %/year (between 30ºS and 30ºN) derived from

508   ACE-FTS data for 2004 to 2010 (Brown et al., 2011).

509   Prior to the calculation of ACE-FTS, HALOE, and SLIMCAT trends, we derived

510   time series as a function of altitude (on the ACE-FTS grid) and latitude (in 10º bins). Figure

511   7 illustrates the ACE-FTS, HALOE and SLIMCAT time series for HF between 1991 and

512   2013 at selected altitudes for six of the latitude bins; for ease of viewing, error bars are not

513   shown. The annual cycle is clearly visible in each time series, a result of the seasonality of

514   the main 'source', COF_2 (Harrison et al., 2014), and careful inspection of Figure 7 reveals

515   that as expected the phase of this cycle is opposite in each hemisphere. The amplitude is

516   largest at high southern latitudes (note the maxima at 29.5 km for the 60˚ - 70˚S plot), due to

517   the descent of HF-rich air in southern winter polar vortices. Note also evidence of the quasi-

518   biennial oscillation (QBO) signal in the tropical plots.

519   Overall the agreement between SLIMCAT and observations presented in Figure 7 is

520   good, however obvious biases are present. In Section 5 it was discussed that ACE v3.0 is

521   biased high relative to HALOE by ~10%. HALOE VMRs are biased low relative to

522   SLIMCAT, generally by between ~5 and 15 %, although SLIMCAT is biased low relative to

523   HALOE by up to ~20 % between ~20 and 30 km in the 0-30˚N region. Additionally, there is

524   a discrepancy in the observed and calculated annual cycle structure over the tropics, e.g. 10˚ -

525   20˚N at 34.5 km. In terms of bias, ACE-FTS v3.0/3.5 data generally agree with SLIMCAT

526   to within ± 5 %, except over much of the lower stratosphere (below 30 km) where SLIMCAT

527   is biased low by at least ~5-15 %, peaking at ~20 % in the 0-30˚N region and ~25-35 % at

528   the southern and northern high latitudes (poleward of 50˚).

529   Figure 8 illustrates the GOZCARDS and SLIMCAT time series for HF plotted in the

530   same manner as Figure 7. Recall that the GOZCARDS HF data product is a merging of the

531   HALOE v19 and ACE-FTS v2.2 HF datasets, with the relative bias between the datasets

532   removed. The agreement between SLIMCAT and the HALOE component of GOZCARDS

533   above ~30 km is reasonably good, however at lower altitudes there are several regions in

534   which the low bias of SLIMCAT is significantly larger than presented in Figure 7, in

535   particular below 20 km near the south pole, and between ~20 and 30 km in the northern

536   hemisphere, where the bias peaks at ~35 % in the 0-30˚N region. The ACE-FTS component

537   of GOZCARDS generally agrees with SLIMCAT to within ± 5 % above 30 km at the tropics

538 and above 25 km in the polar regions. At altitudes lower than these SLIMCAT is biased low,

539 for example by ~5 – 10 % at latitudes above 50 ˚N and up to 25 % lower between 20 and 30

540 km in the 0-30˚N region.

541   The GOZCARDS merging process for HF relied only on the relative bias between

542 the HALOE v19 HF and ACE-FTS v2.2 HF datasets. In this study, it is not possible to

543 comment on systematic or absolute biases. However, regardless of the absolute biases of the

544 various datasets, it is clear that SLIMCAT tends to consistently underestimate HF VMRs at

545 low altitudes (below 30 km at the tropics and 25 km at the poles) relative to those at higher

546 altitudes.

547   HF trends for the ACE-FTS, HALOE, and SLIMCAT time series (trends were not

548 considered for GOZCARDS as this is a merged dataset directly related in a multiplicative

549 fashion to the original datasets) at each altitude within each latitude bin have been calculated

550 for three time periods from monthly percentage anomalies in HF zonal means, $C^{z,\theta}(n)$,

551 defined as

552
$$C^{z,\theta}(n) = 100 \frac{VMR^{z,\theta}(n) - \sum_{m=1}^{12} \delta_{nm} \overline{VMR}^{z,\theta}(m)}{\sum_{m=1}^{12} \delta_{nm} \overline{VMR}^{z,\theta}(m)}, \qquad (7)$$

553 where n is a running index from month zero to month n-1, $VMR^{z,\theta}(n)$ is the corresponding

554 mixing ratio at altitude z and latitude θ, $\overline{VMR}^{z,\theta}(m)$ is the average of all zonal means for each

555 of the twelve months, m, and δ_{nm}, although not used in its strict mathematical sense, is one

556 when index n corresponds to one of the months m and is zero otherwise (Harrison et al.,

557 2014). Such an approach essentially removes the annual cycle and the effect of biases in

558 VMRs; the trend, in units of %/year, is simply equated to the 'slope' of the linear regression

559 between $C^{z,\theta}(n)$ and the dependent variable $n/12$. The inclusion of additional terms such as

560 the annual cycle and its harmonics resulted in no additional improvement in the regression.

561 The three time periods considered are January 2004 to December 2012 (ACE-FTS,

562 SLIMCAT), October 1991 to December 1997 (HALOE, SLIMCAT), and January 1998 to

563 November 2005 (HALOE, SLIMCAT). The HALOE time series was split into two periods

564 for which HF growth could be modelled linearly. Errors have been explicitly treated in the

565 linear regression of the ACE and HALOE data, but not the SLIMCAT outputs.

566   Figure 9 presents the trends in the growth of HF (percent per year) (January 2004 to

567 December 2012) for ACE and SLIMCAT as a function of latitude and altitude, up to the top

568 of the ACE-FTS retrieval range. The ACE-FTS plot in Figure 9 indicates that between 2004

17

569   and 2012, HF has increased most rapidly (2 – 3 %/year) at altitudes below ~25 km in the

570   northern hemisphere and at ~35 km near the equator. Similarly, HF has decreased most

571   rapidly in the southern hemisphere below ~35 km and in the northern hemisphere between ~

572   30 and 35 km. The SLIMCAT plot in the second panel contains a number of features which

573   agree well with those in the ACE plot. In particular, note the region of negative trends in the

574   southern hemisphere below ~30 – 35 km, peaking at -3.5 – -4.0 %/year, the region of high

575   positive trends in the northern hemisphere below ~30 km, peaking at 4.5 – 5.0 %/year, the

576   small region of positive trend at ~35 km near the equator, peaking at 2.0 – 2.5 %/year, and

577   the slightly larger region of negative trend at ~30 – 40 km at 0˚ to 30˚N, peaking at -1.0 – -

578   1.5 %/year. However, the magnitudes of the SLIMCAT trends in the lower stratosphere are

579   biased high compared with the ACE measurements.

580   An additional SLIMCAT run has been performed with dynamics arbitrarily annually

581   repeating those for the year 2000; results from this run give a 'clean' HF signal without the

582   complication of changes in stratospheric dynamics. Results from this run are included in the

583   times series plots in Figure 7; the annual repetition in dynamical structure reveals a clearer

584   signal of the long-term chemical changes. 'Clean' HF trends for 2004 – 2012 calculated in

585   the same manner as before are plotted in the lowest panel of Figure 9, revealing trends

586   distributed relatively uniformly throughout the stratosphere with values between 0 and 1

587   %/year. This indicates that the variations in trends observed for the full SLIMCAT run result

588   from changes in stratospheric dynamics over the observation period. The information on

589   stratospheric circulation is provided solely by the analyses used to force the SLIMCAT

590   calculations. Similar changes due to stratospheric dynamics were observed for COF_2

591   (Harrison et al., 2014). Moreover, Ploeger et al. (2015) used a Lagrangian chemical transport

592   model, also forced by ECMWF ERA-Interim reanalyses, to look at variations in stratospheric

593   age-of-air (AoA) over the period 1988-2013. They compared their model results with

594   estimates derived from MIPAS satellite observations for 2002-2012. During the period of

595   MIPAS observations they found that stratospheric AoA decreased in the lower stratosphere

596   but showed interhemispheric differences in the trend above about 20 km. Also, despite the

597   ongoing monotonic decrease of near-surface chlorine source gases, recent ground-based and

598   satellite remote-sensing measurements have shown a significant increase in hydrogen

599   chloride (HCl), the main stratospheric chlorine reservoir, in the lower stratosphere of the

600   Northern Hemisphere between 2007 and 2011 (Mahieu et al., 2014). By comparison to

601   similar SLIMCAT simulations as used here, this trend 'anomaly' was attributed to multiyear

602   variability in the stratospheric circulation and dynamics.

18

603   Together, the studies discussed above paint a consistent picture whereby variability

604   in stratospheric transport, which varies with altitude and hemisphere, significantly modifies

605   the observed trends in long-lived tracers. This variability seems to be well captured by

606   reanalysis products such as ERA-Interim. Even if these tracers have monotonic VMR trends

607   in the troposphere, this dynamical variability can lead to complicated behaviour in the

608   stratosphere and must therefore be accounted for when using observations to determine

609   underlying chemical trends. A detailed analysis of the changing stratospheric dynamics that

610   are responsible for the observed trends in HF and other species is beyond the scope of this

611   work and would require a coupled chemistry-dynamical model.

612   Trends have similarly been derived for the two HALOE periods. HALOE plots

613   corresponding to the ACE-FTS plots in Figure 9 can be found in Figures 10 (1991 – 1997)

614   and 11 (1998 – 2005). The HALOE trends in Figure 10 peaking in the northern hemisphere

615   between 0˚ and 40˚N broadly agree with those calculated by SLIMCAT in the same region,

616   however SLIMCAT calculates smaller trends at the lowest altitudes and generally

617   underestimates the trends in the southern hemisphere. The differences between the full and

618   fixed-dynamics SLIMCAT runs show the impact of dynamical variability; the fixed-

619   dynamics run provides a clean chemical signal. Of the three periods considered, the

620   comparison between 1991 – 1997 HALOE trends and those calculated from SLIMCAT is the

621   poorest. The North-South asymmetry in trends for the full SLIMCAT calculation, which

622   does not agree with observations, must be due to dynamical variability in the model, with the

623   dynamics imposed solely by the ECMWF analyses. Over the measurement period, the

624   quality of these analyses may vary depending on the available datasets used for the

625   assimilation, but it is very difficult to test how realistic the stratospheric transport is. There

626   are only a handful of other height-resolved datasets that test this aspect of the stratospheric

627   circulation, e.g. ozone (Dhomse et al., 2015). As evidenced by Figure 11, however, the

628   HALOE trends for 1998 – 2005 agree better with SLIMCAT than for the 1991 – 1997 period,

629   with 'background' trends generally between 0.5 and 1.5 %/year. In fact, there is very little

630   variability over the majority of the plotted range.

631   Overall global trends in HF, weighted at each altitude and latitude by $\cos^2$(latitude˚)

632   and the average VMR, have been calculated from the three time series using errors

633   determined from the linear regression; these trends are listed in Table 5. The observed HF

634   trends reveal a substantial slowing down in the rate of increase of HF by ~90 % from the

635   mid-1990s over the next 15 years, namely from 4.97 ± 0.12 %/year (1991-1997) to 1.12 ±

636   0.08 %/year (1998-2005) to 0.52 ± 0.03 %/year (2004-2012). In addition to direct

637 stratospheric ozone recovery (e.g. Chipperfield et al., 2015), this marked decline in the
638 growth rate of HF is a particularly important marker for the success of the Montreal Protocol,
639 and should drop even further once HCFC-22 is phased out in developing countries over the
640 coming years. Global trends calculated by SLIMCAT for the HALOE (1998 – 2005) and
641 ACE-FTS (2004 – 2012) time series, 1.10 %/year and 0.48 %/year, respectively, agree very
642 well with observations, however for the 1991 – 1997 HALOE period the model produces a
643 value ~20 % lower (4.01 %/year). Again, the reason for this is not completely clear, but is
644 likely related to the ECMWF analysis used to drive the dynamics in the SLIMCAT
645 calculation.

646

647 **7. Conclusions**

648   Hydrogen fluoride (HF) is the most abundant fluorine reservoir in the stratosphere
649 with main sources arising from the atmospheric degradation of CFC-12 (CCl_2F_2), CFC-11
650 (CCl_3F), HCFC-22 ($CHClF_2$), and CFC-113 (CCl_2FCClF_2), ozone-depleting species whose
651 emissions are anthropogenic. Monitoring the growth of stratospheric HF is therefore an
652 important marker for the success of the Montreal Protocol.

653   Global distributions and trends of stratospheric HF have been determined from
654 ACE-FTS (2004 –) and HALOE (1991 – 2005) data. Based on the overlap period between
655 datasets, ACE-FTS HF measurements are biased high by ~10% relative to HALOE. The
656 observations have been compared with the output of SLIMCAT, a three-dimensional CTM,
657 and the agreement is generally good, although SLIMCAT tends to underestimate HF VMRs
658 at low altitudes (below 30 km at the tropics and 25 km at the poles) relative to those at higher
659 altitudes.

660   The observed global HF trends reveal a substantial slowing down in the rate of
661 increase of HF since the 1990s: 4.97 ± 0.12 %/year (1991-1997; HALOE), 1.12 ± 0.08
662 %/year (1998-2005; HALOE), and 0.52 ± 0.03 %/year (2004-2012; ACE-FTS), indicating
663 the effectiveness of the Montreal Protocol in phasing out the principal precursor species. For
664 the same periods, SLIMCAT calculates trends of 4.01 %/year, 1.10 %/year, and 0.48 %/year,
665 respectively. The observations also reveal variations in the HF trends with latitude and
666 altitude, for example between 2004 and 2012 HF actually decreased in the southern
667 hemisphere below ~35 km. SLIMCAT calculations broadly agree with these observations,
668 most notably between 2004 and 2012. Such variations are attributed to variability in
669 stratospheric dynamics over the observation period.

670   The ACE-FTS is the only satellite instrument currently making measurements of
671 HF, and continues to operate with only minor loss in performance since its launch. It will
672 therefore be possible to extend the HF time series to the present day and beyond, and
673 subsequently extend the comparison with SLIMCAT.
674

675 **Author contribution**
676   J. J. Harrison devised the study and performed the data analysis. C. D. Boone and P.
677 F. Bernath provided the ACE-FTS data. J. Russell III provided the HALOE HF data. L.
678 Froidevaux and J. Anderson provided the HF GOZCARDS data. M. P. Chipperfield and S.
679 S. Dhomse ran the SLIMCAT model and provided additional explanation of the outputs. J. J.
680 Harrison prepared the manuscript with contributions from M. P. Chipperfield and the other
681 co-authors.
682

693 **Figure Captions**
694

695 **Figure 1**. A comparison between ACE-FTS and SLIMCAT HF zonal means (September
696 2009 to August 2010). A full discussion of the seasonal variation in the HF distribution is
697 provided in the text.
698

699 **Figure 2**. A comparison between ACE-FTS, HALOE and SLIMCAT HF zonal means
700 (September 2004 to August 2005). The ACE-FTS and HALOE time series of measurements
701 overlap during the period January 2004 to November 2005.
702

Figure 3. A comparison of COF_2 and $COClF$ zonal means from ACE-FTS and SLIMCAT for October 2009, and February and August 2010.

Figure 4. Correlation plots between coincident CFC-12 and COF_2 ACE-FTS observations and SLIMCAT calculations for November 2009 / July 2010 65-70ºS and January / May 2010 65-70ºN. The error bars represent the standard deviations in the ACE-FTS VMRs.

Figure 5. Correlation plots between coincident CFC-11 and $COClF$ ACE-FTS observations and SLIMCAT calculations for November 2009 / July 2010 65-70ºS and January / May 2010 65-70ºN. The error bars represent the standard deviations in the ACE-FTS VMRs.

Figure 6. Correlation plots between coincident ACE-FTS observations and SLIMCAT calculations of total 'major' organic fluorine, based on CFC-11, CFC-12, and HCFC-22, and total inorganic fluorine, F_y, for November 2009 / July 2010 65-70ºS and January / May 2010 65-70ºN. The error bars represent the standard deviations in the ACE-FTS VMRs.

Figure 7. The HALOE, ACE-FTS and SLIMCAT HF time series for selected altitude – latitude bin combinations. Observations are plotted between October 1991 and December 2012. Overlaid are the time series from a SLIMCAT run with dynamics arbitrarily annually repeating those for the year 2000; this provides a clearer signal of the long-term chemical changes without the complication of variations in stratospheric dynamics.

Figure 8. The GOZCARDS and SLIMCAT HF time series for selected altitude – latitude bin combinations. Observations are plotted between October 1991 and September 2010.

Figure 9. Trends in the growth of HF (% yr^{-1}; January 2004 to December 2012) for ACE-FTS and SLIMCAT as a function of latitude and altitude. A full discussion of these trends is provided in the text.

Figure 10. Trends in the growth of HF (% yr^{-1}; October 1991 to December 1997) for HALOE and SLIMCAT as a function of latitude and altitude. A full discussion of these trends is provided in the text.

22

736 **Figure 11**. Trends in the growth of HF (% yr^{-1}; January 1998 to November 2005) for
737 HALOE and SLIMCAT as a function of latitude and altitude. A full discussion of these
738 trends is provided in the text.
739
740 **References**
741

742 Bernath, P. F., McElroy, C. T., Abrams, M. C., Boone, C. D., Butler, M., Camy-Peyret, C.,
743 Carleer, M., Clerbaux, C., Coheur, P.-F., Colin, R., DeCola, P., DeMazière, M., Drummond,
744 J. R., Dufour, D., Evans, W. F. J., Fast, H., Fussen, D., Gilbert, K., Jennings, D.E.,
745 Llewellyn, E. J., Lowe, R. P., Mahieu, E., McConnell, J. C., McHugh, M., McLeod, S. D.,
746 Michaud, R., Midwinter, C., Nassar, R., Nichitiu, F., Nowlan, C., Rinsland, C. P., Rochon, Y.
747 J., Rowlands, N., Semeniuk, K., Simon, P., Skelton, R., Sloan, J. J., Soucy, M.-A., Strong,
748 K., Tremblay, P., Turnbull, D., Walker, K. A., Walkty, I., Wardle, D. A., Wehrle, V., Zander,
749 R., and Zou, J.: Atmospheric Chemistry Experiment (ACE): Mission overview, Geophys.
750 Res. Lett., 32, L15S01, doi:10.1029/2005GL022386, 2005.
751
752 Boone, C. D., Walker, K. A., Bernath, P. F.: Version 3 Retrievals for the Atmospheric
753 Chemistry Experiment Fourier Transform Spectrometer (ACE-FTS). In The Atmospheric
754 Chemistry Experiment ACE at 10: A Solar Occultation Anthology; Bernath, P. F., Ed.; A.
755 Deepak Publishing, Hampton, Virginia, U.S.A., 103-127, 2013. Available at
756 http://www.ace.uwaterloo.ca/publications/2013/Version3.5retreivals2013.pdf.
757
758 Brown, A. T., Chipperfield, M. P., Boone, C., Wilson, C., Walker, K. A., Bernath, P. F.:
759 Trends in atmospheric halogen containing gases since 2004, J. Quant. Spectrosc. Rad. Trans.,
760 112, 2552-2566, 2011.
761
762 Brown, A. T., Chipperfield, M. P., Richards, N. A. D., Boone, C., and Bernath, P. F.: Global
763 stratospheric fluorine inventory for 2004–2009 from Atmospheric Chemistry Experiment
764 Fourier Transform Spectrometer (ACE-FTS) measurements and SLIMCAT model
765 simulations, Atmos. Chem. Phys., 14, 267-282, doi:10.5194/acp-14-267-2014, 2014.
766
767 Chipperfield, M. P.: Multiannual simulations with a three-dimensional chemical transport
768 model, J. Geophys. Res., 104, 1781–1805, doi:10.1029/98jd02597, 1999.
769

770 Chipperfield, M. P.: New version of the TOMCAT/SLIMCAT off-line chemical transport
771 model: Intercomparison of stratospheric tracer experiments, Q. J. R. Meteorol. Soc., 132,
772 1179–1203, 2006.

773

774 Chipperfield, M. P., Liang, Q., Strahan, S. E., Morgenstern, O., Dhomse, S. S., Abraham, N.
775 L., Archibald, A. T., Bekki, S., Braesicke, P., Di Genova, G., Fleming, E. L., Hardiman, S.
776 C., Iachetti, D., Jackman, C. H., Kinnison, D. E., Marchand, M., Pitari, G., Pyle, J. A.,
777 Rozanov, E., Stenke, A., Tummon, F.: Multimodel estimates of atmospheric lifetimes of
778 long-lived ozone-depleting substances: Present and future, J. Geophys. Res. Atmos., 119,
779 2555–2573, doi:10.1002/2013JD021097, 2014.

780

781 Chipperfield, M.P., Dhomse, S.S., Feng, W., McKenzie, R.L., Velders, G., Pyle, J.A.:
782 Quantifying the ozone and UV benefits already achieved by the Montreal Protocol, Nature
783 Communications, 6, 7233, doi:10.1038/ncomms8233, 2015.

784

785 Connor, B. J., and Rodgers, C. D.: A comparison of retrieval methods: Optimal estimation,
786 onion peeling, and a combination of the two, in RSRM 1987: Advances in Remote Sensing
787 Retrieval Methods; edited by Deepak, A., Fleming, H. E., and Theon, J. S., Eds.; A. Deepak
788 Publishing, Hampton, Virginia, U.S.A., 1989.

789

790 Dhomse, S., Chipperfield, M.P., Feng, W., Hossaini, R., Mann, G.W., Santee, M.L.:
791 Revisiting the hemispheric asymmetry in mid-latitude ozone changes following the Mount
792 Pinatubo eruption: A 3-D model study, Geophys. Res. Lett., 42, 3038-3047,
793 doi:10.1002/2015GL063052, 2015.

794

795 Duchatelet, P., Demoulin, P., Hase, F., Ruhnke, R., Feng, W., Chipperfield, M. P., Bernath,
796 P. F., Boone, C. D., Walker, K. A., and Mahieu, E.: Hydrogen fluoride total and partial
797 column time series above the Jungfraujoch from long-term FTIR measurements: Impact of
798 the line-shape model, characterization of the error budget and seasonal cycle, and comparison
799 with satellite and model data, J. Geophys. Res., 115, D22306, doi:10.1029/2010JD014677,
800 2010.

801

802 Feng, W., Chipperfield, M. P., Dorf, M., Pfeilsticker, K., and Ricaud, P.: Mid-latitude ozone
803 changes: studies with a 3-D CTM forced by ERA-40 analyses, Atmos. Chem. Phys., 7, 2357–
804 2369, doi:10.5194/acp-7-2357-2007, 2007.

805

806 Froidevaux, L., Anderson, J., Wang, H.-J., Fuller, R. A., Schwartz, M. J., Santee, M. L.,
807 Livesey, N. J., Pumphrey, H. C., Bernath, P. F., Russell III, J. M., and McCormick, M. P.:
808 Global OZone Chemistry And Related trace gas Data records for the Stratosphere
809 (GOZCARDS): methodology and sample results with a focus on HCl, H_2O, and O_3, Atmos.
810 Chem. Phys., 15, 10471-10507, doi:10.5194/acp-15-10471-2015, 2015.

811

812 Fu, D., Boone, C. D., Bernath, P. F., Weisenstein, D. K., Rinsland, C. P., Manney, G. L.,
813 Walker, K. A.   First global observations of atmospheric COClF from the Atmospheric
814 Chemistry Experiment mission, J. Quant. Spectrosc. Rad. Trans., 110, 974–985, 2009.

815

816 Gribble, G. W. Naturally Occurring Organofluorines. In Handbook of Environmental
817 Chemistry, Vol.3, Part N: Organofluorines; Neilson, A. H., Ed.; Springer-Verlag: Berlin
818 Heidelberg, 2002.

819

820 Harrison, J. J., Chipperfield, M. P., Dudhia, A., Cai, S., Dhomse, S., Boone, C. D., and
821 Bernath, P. F.: Satellite observations of stratospheric carbonyl fluoride, Atmos. Chem. Phys.,
822 14, 11915-11933, doi:10.5194/acp-14-11915-2014, 2014.

823

824 Irion F.W., Gunson M.R., Toon G.C., Chang A.Y., Eldering A., Mahieu E., Manney G.L.,
825 Michelsen H.A., Moyer E.J., Newchurch M.J., Osterman G.B., Rinsland C.P., Salawitch R.J.,
826 Sen B., Yung Y.L., Zander R., Atmospheric Trace Molecule Spectroscopy (ATMOS)
827 Experiment Version 3 data retrievals, Appl Opt. 2002 Nov 20;41(33):6968-79.

828

829 Kohlhepp, R., Ruhnke, R., Chipperfield, M. P., De Mazière, M., Notholt, J., Barthlott, S.,
830 Batchelor, R. L., Blatherwick, R. D., Blumenstock, Th., Coffey, M. T., Demoulin, P., Fast,
831 H., Feng, W., Goldman, A., Griffith, D. W. T., Hamann, K., Hannigan, J. W., Hase, F.,
832 Jones, N. B., Kagawa, A., Kaiser, I., Kasai, Y., Kirner, O., Kouker, W., Lindenmaier, R.,
833 Mahieu, E., Mittermeier, R. L., Monge-Sanz, B., Morino, I., Murata, I., Nakajima, H., Palm,
834 M., Paton-Walsh, C., Raffalski, U., Reddmann, Th., Rettinger, M., Rinsland, C. P., Rozanov,
835 E., Schneider, M., Senten, C., Servais, C., Sinnhuber, B.-M., Smale, D., Strong, K.,

836 Sussmann, R., Taylor, J. R., Vanhaelewyn, G., Warneke, T., Whaley, C., Wiehle, M., and
837 Wood, S. W.: Observed and simulated time evolution of HCl, ClONO$_2$, and HF total column
838 abundances, Atmos. Chem. Phys., 12, 3527-3556, doi:10.5194/acp-12-3527-2012, 2012.

839

840 Mahieu, E., Duchatelet, P., Demoulin, P., Walker, K. A., Dupuy, E., Froidevaux, L., Randall,
841 C., Catoire, V., Strong, K., Boone, C. D., Bernath, P. F., Blavier, J.-F., Blumenstock, T.,
842 Coffey, M., De Mazière, M., Griffith, D., Hannigan, J., Hase, F., Jones, N., Jucks, K. W.,
843 Kagawa, A., Kasai, Y., Mebarki, Y., Mikuteit, S., Nassar, R., Notholt, J., Rinsland, C. P.,
844 Robert, C., Schrems, O., Senten, C., Smale, D., Taylor, J., Tétard, C., Toon, G. C., Warneke,
845 T., Wood, S. W., Zander, R., and Servais, C.: Validation of ACE-FTS v2.2 measurements of
846 HCl, HF, CCl$_3$F and CCl$_2$F$_2$ using space-, balloon- and ground-based instrument
847 observations, Atmos. Chem. Phys., 8, 6199-6221, doi:10.5194/acp-8-6199-2008, 2008.

848

849 Mahieu, E., Chipperfield, M. P., Notholt, J., Reddmann, T., Anderson, J., Bernath, P. F.,
850 Blumenstock, T., Coffey, M. T., Dhomse, S. S., Feng, W., Franco, B., Froidevaux, L.,
851 Griffith, D. W. T., Hannigan, J. W., Hase, F., Hossaini, R., Jones, N. B., Morino, I., Murata,
852 I., Nakajima, H., Palm, M., Paton-Walsh, C., Russell III, J. M., Schneider, M., Servais, C.,
853 Smale, D., and Walker, K. A: Recent Northern Hemisphere stratospheric HCl increase due to
854 atmospheric circulation changes, Nature, 515, 104-107, doi:10.1038/nature13857, 2014.

855

856 Monge-Sanz, B. M., Chipperfield, M. P., Simmons, A. J., and Uppala, S. M.: Mean age of air
857 and transport in a CTM: Comparison of different ECMWF analyses, Geophys. Res. Lett., 34,
858 L04801, doi:10.1029/2006gl028515, 2007.

859

860 Perrin, A., Demaison, J., and Toon, G.: The ν_1, ν_2, and ν_3 bands of carbonyl chlorofluoride
861 (COFCl) at 5.3, 9.1, and 13.1 μm: position and intensity parameters and their use for
862 atmospheric studies, J. Quant. Spectrosc. Rad. Trans., 112, 1266-1279,
863 10.1016/j.jqsrt.2011.01.003, 2011.

864

865 Ploeger, F., Riese, M., Haenel, F., Konopka, P., Müller, R. and Stiller, G.: Variability of
866 stratospheric mean age of air and of the local effects of residual circulation and eddy mixing,
867 J. Geophys. Res. Atmos., 120, 716–733, doi:10.1002/2014JD022468, 2015.

868

869 Plumb, R. A. and Ko, M. K. W.: Interrelationships between mixing ratios of long-lived
870 stratospheric constituents, J. Geophys. Res., 97, 10145–10156, 1992.

871

872 Ricaud, P., and Lefevre, F.: Fluorine in the atmosphere. In Fluorine and the Environment:
873 Atmospheric Chemistry, Emissions, & Lithosphere; Tressaud, A., ed., Elsevier, 2006.

874

875 Rothman, L.S., Gamache, R.R., Tipping, R.H., Rinsland, C.P., Smith, M.A.H., Benner D. C.,
876 Devi, V.M, Flaud, J.-M., Camy-Peyret, C., Perrin, A., Goldman, A., Massie, S.T., Brown,
877 L.R., Toth, R.A.: The HITRAN molecular database: Editions of 1991 and 1992, J. Quant.
878 Spectrosc. Radiat. Transfer, 48, 469–507, 1992.

879

880 Rothman, L.S., Jacquemart, D., Barbe, A., Benner, C. D., Birk, M., Brown, L. R., Carleer, M.
881 R., Chackerian Jr., C., Chance, K., Coudert, L. H., Dana, V., Devi, V. M., Flaud, J.-M.,
882 Gamache, R. R., Goldman, A., Hartmann, J.-M., Jucks, J. W., Maki, A. G., Mandin, J.-Y.,
883 Massie, S. T., Orphal, J., Perrin, A., Rinsland, C. P., Smith, M., Tennyson, J., Tolchenov, R.
884 N., Toth, R. A., Vander Auwera, J., Varanasi, P., and Wagner, G.: The HITRAN 2004
885 molecular spectroscopic database, J. Quant. Spectrosc. Radiat. Transfer, 96, 193–204, 2005.

886

887 Rothman, L.S., Gordon, I.E., Babikov, Y., Barbe, A., Benner, D.C., Bernath, P.F., Birk, M.,
888 Bizzocchi, L., Boudon, V., Brown, L.R., Campargue, A., Chance, K., Cohen, E.A., Coudert,
889 L.H., Devi, V.M., Drouin, B.J., Fayt, A., Flaud, J.-M., Gamache, R.R., Harrison, J.J.,
890 Hartmann, J.-M., Hill, C., Hodges, J.T., Jacquemart, D., Jolly, A., Lamouroux, J., Le Roy,
891 R.J., Li, G., Long, D.A., Lyulin, O.M., Mackie, C.J., Massie, S.T., Mikhailenko, S., Müller,
892 H.S.P., Naumenko, O.V., Nikitin, A.V., Orphal, J., Perevalov, V., Perrin, A., Polovtseva,
893 E.R., Richard, C., Smith, M.A.H., Starikova, E., Sung, K., Tashkun, S., Tennyson, J., Toon,
894 G.C., Tyuterev, Vl.G., Wagner, G.: The HITRAN2012 molecular spectroscopic database, J.
895 Quant. Spectrosc. Radiat. Transfer, 130, 4-50, 2013.

896

897 Russell III, J. M., Gordley, L. L., Park, J. H., Drayson, S. R., Hesketh, W. D., Cicerone, R. J.,
898 Tuck, A. F., Frederick, J. E., Harries, J. E., Crutzen, P. J.: The Halogen Occultation
899 Experiment, J. Geophys. Res., 98, 10777-10797, doi:10.1029/93JD00799, 1993.

900

901 Russell III, J. M., Deaver, L. E., Luo, M., Cicerone, R. J., Park, J. H., Gordley, L. L., Toon,
902 G. C., Gunson, M. R., Traub, W. A., Johnson, D. G., Jucks, K. W., Zander, R. and Nolt, I. G.:

903   Validation of hydrogen fluoride measurements made by the Halogen Occultation Experiment

904   from the UARS platform, J. Geophys. Res., 101, 10163–10174, 1996.

905

906   Velazco, V. A., Toon, G. C., Blavier, J.-F. L., Kleinböhl, A., Manney, G. L., Daffer, W. H.,

907   Bernath, P. F., Walker, K. A., and Boone, C.: Validation of the Atmospheric Chemistry

908   Experiment by noncoincident MkIV balloon profiles, J. Geophys. Res., 116, D06306,

909   doi:10.1029/2010jd014928, 2011.

910

911   Zander, R., Roland, G. and Delbouille, L.: Confirming the presence of hydrofluoric acid in

912   the upper stratosphere, Geophys. Res. Lett., 4, 117–120, 1977.

913

914   Zander, R., Roland, G., Delbouille, L., Sauval, A., Farmer, C.B., Norton, R.H.: Monitoring of

915   the integrated column of hydrogen fluoride above the Jungfraujoch Station since 1977 — the

916   HF/HCl column ratio, Journal of Atmospheric Chemistry, 5, 385-394, 1987.

917

918

919   **Tables**

920

921   Table 1: Microwindows for the v3.0/v3.5 ACE-FTS hydrogen fluoride retrieval.

Centre Frequency (cm^{-1})	Microwindow width (cm^{-1})	Lower altitude (km)	Upper altitude (km)
3787.60	1.60	40	2.00E+16[b]
3788.28	0.60	12	40
3792.65[a]	0.40	20	40
3833.70	0.80	16	40
3834.30	1.60	40	9.00E+15[b]
3877.60	0.80	12	9.00E+15[b]
3920.15	0.70	25	9.00E+15[b]
4000.87	0.65	12	9.00E+15[b]
4038.82	1.00	12	9.00E+15[b]
4075.35	0.80	25	9.00E+15[b]
4109.75	0.80	25	2.00E+16[b]

922   [a] Included to improve results for interferer HDO.

923   [b] Upper altitude given in atmospheric density units, molecules cm^{-3}.

924

925

926   Table 2: Interferers in the v3.0/v3.5 ACE-FTS hydrogen fluoride retrieval.

Molecule	Lower altitude limit (km)	Upper altitude limit (km)
H_2O	12	65
$H^{18}OH$	12	50
$H^{17}OH$	12	40
HDO	12	25
CO_2	12	40
O_3	12	38
CH_4	12	30
$OC^{18}O$	12	20
N_2O	12	30

927

928

929 Table 3: Sources of systematic uncertainty in the ACE-FTS v3.0/v3.5 hydrogen fluoride
930 retrieval.

Source	Symbol	Fractional value
HF spectroscopy	μ_{spec}	0.04
Spectral interferers	μ_{int}	0.01
Temperature	μ_T	0.01
Altitude	μ_z	0.03
ILS	μ_{ILS}	0.09

931

932 Table 4: Fluorine source gases in the SLIMCAT chemical scheme and their atmospheric
933 degradation products.

Source gases		Product gases
Commercial name	Chemical formula	
CFC-11	CCl_3F	$COClF$
CFC-12	CCl_2F_2	COF_2
CFC-113	CCl_2FCClF_2	$COClF + COF_2$
CFC-114	$CClF_2CClF_2$	$2COF_2$
CFC-115	$CClF_2CF_3$	$2COF_2 + HF$
HCFC-22	$CHClF_2$	COF_2
HCFC-141b	CH_3CCl_2F	$COClF$
HCFC-142b	CH_3CClF_2	COF_2
HFC-23	CHF_3	$COF_2 + HF$
HFC-134a	CH_2FCF_3	$COF_2 + 2HF$
HFC-152a	CH_3CHF_2	$2COF_2$
Halon 1211	$CBrClF_2$	COF_2
Halon 1301	$CBrF_3$	$COF_2 + HF$
Halon 2402	$CBrF_2CBrF_2$	$4HF$
$COClF^a$		HF
$COF_2{}^a$		$2HF$

934 [a] These are not source gases, but their degradation products are included for completion.

935

936 Table 5: Trends (%/year) derived from the HALOE v19 and ACE-FTS v3.0/v3.5 HF
937 observations.

Dataset	Period	Observed trend	SLIMCAT trend
HALOE	1991-1997	4.97 ± 0.12	4.01
HALOE	1998-2005	1.12 ± 0.08	1.10
ACE-FTS	2004-2012	0.52 ± 0.03	0.48

938

ACE COF₂ 02/2010   SLIMCAT COF₂ 02/2010   ACE COCIF 02/2010   SLIMCAT COCIF 02/2010

ACE COF₂ 08/2010   SLIMCAT COF₂ 08/2010   ACE COCIF 08/2010   SLIMCAT COCIF 08/2010

COF₂ VMR (ppt)

COCIF VMR (ppt)
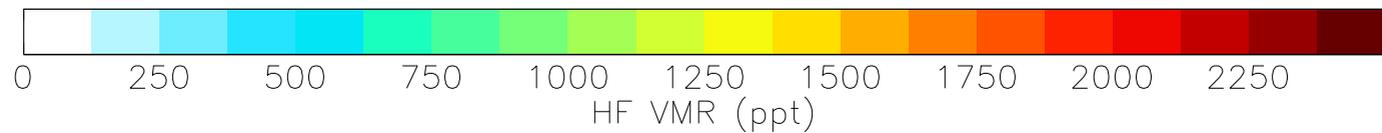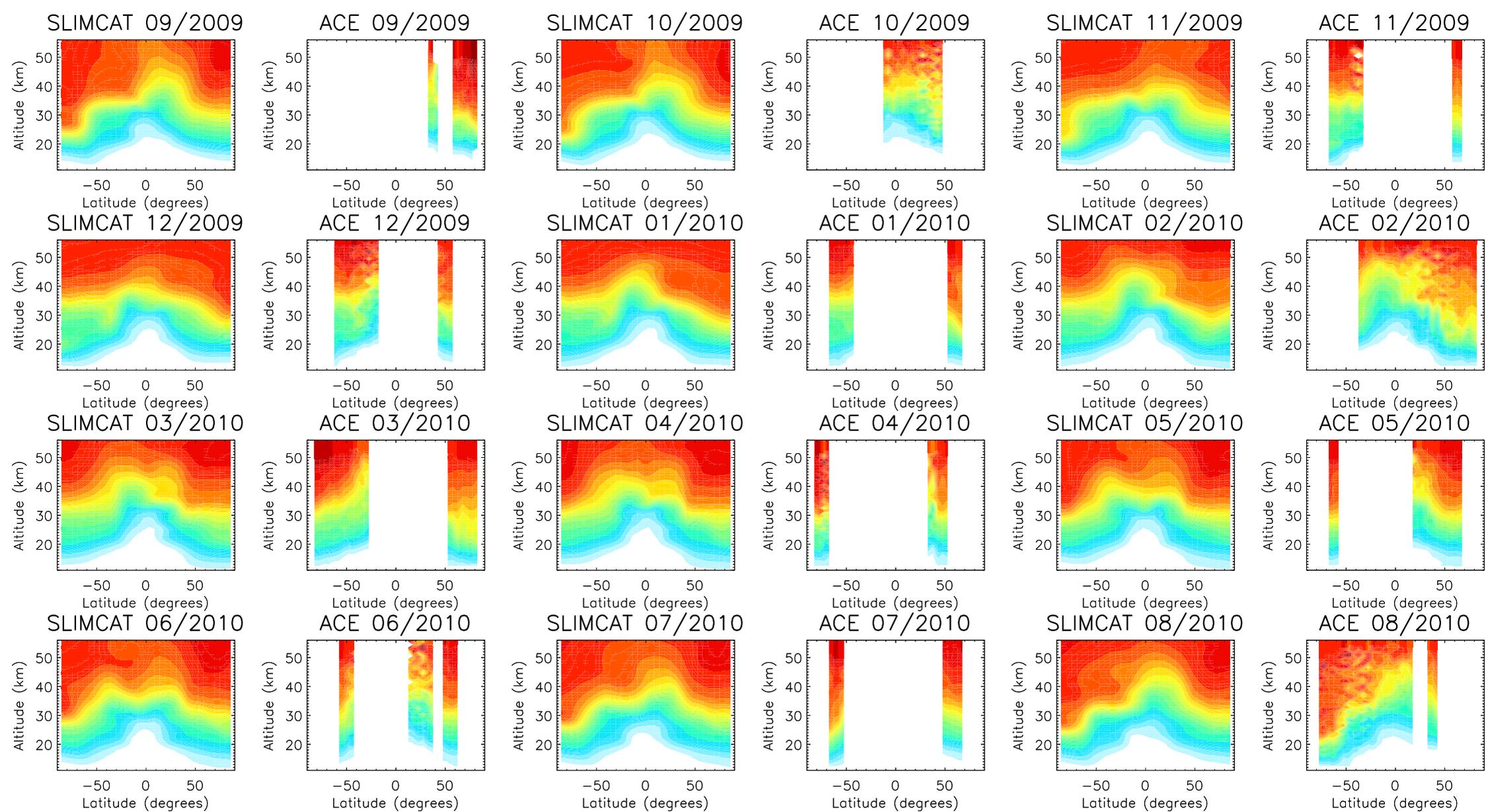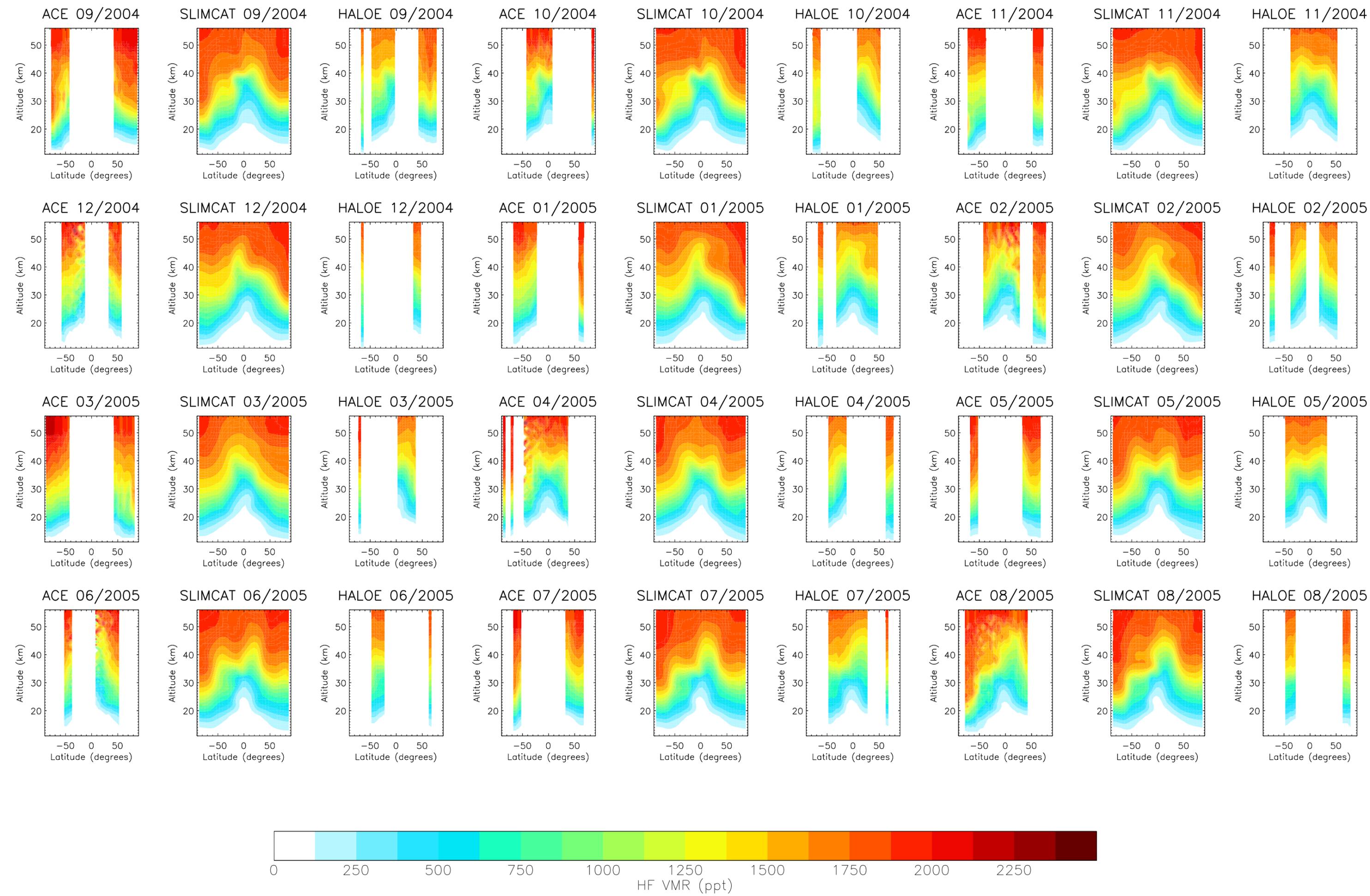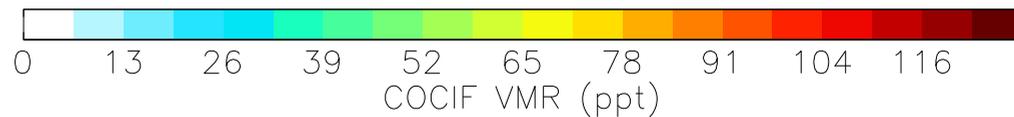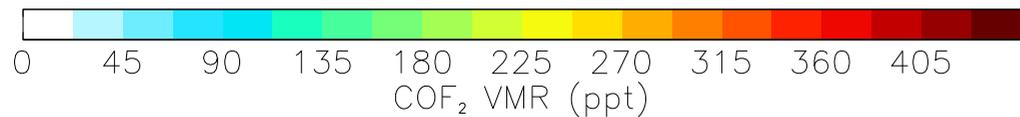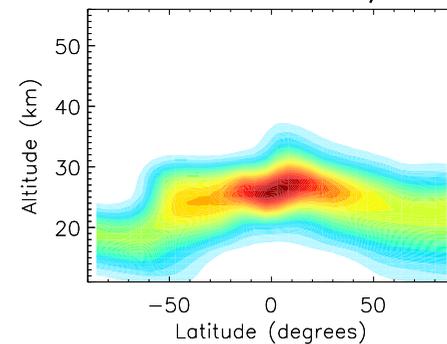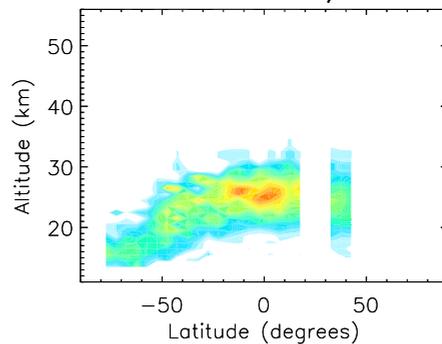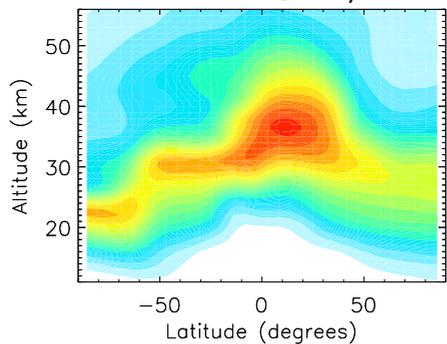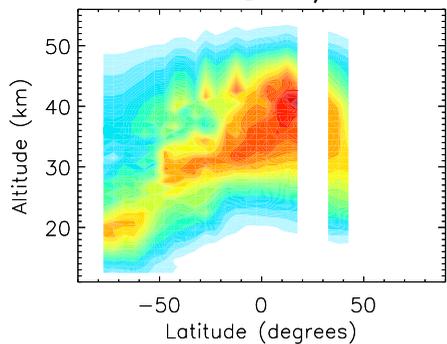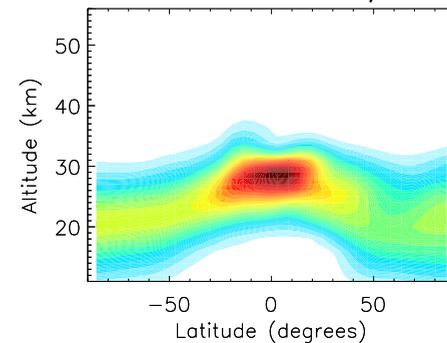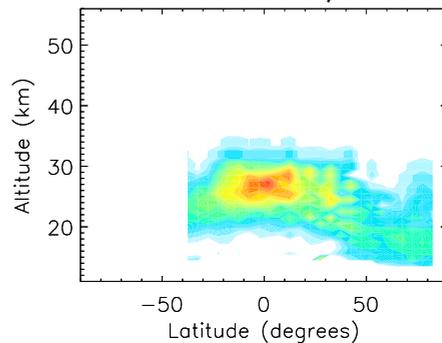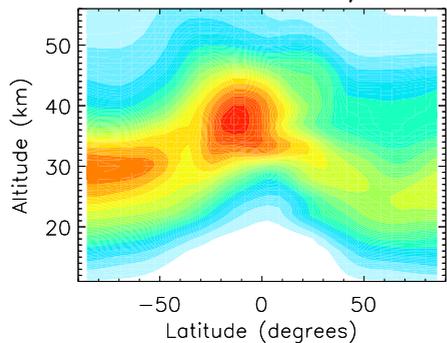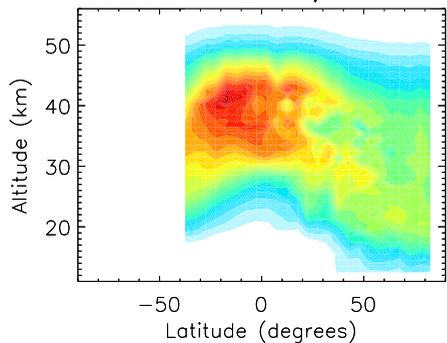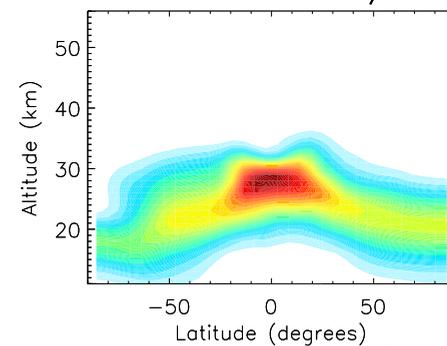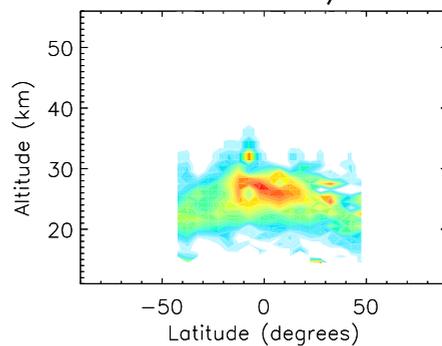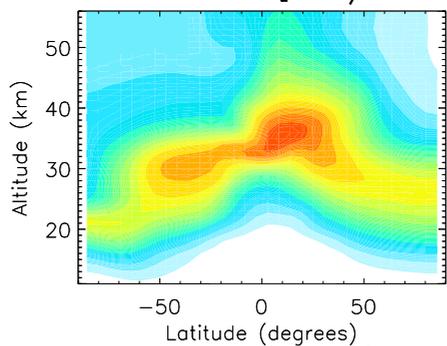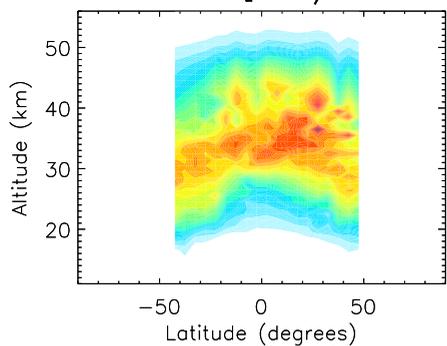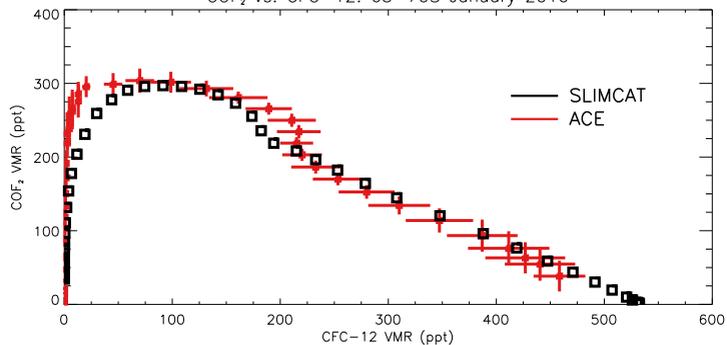
COCIF vs. CFC-11: 65-70N November 2009
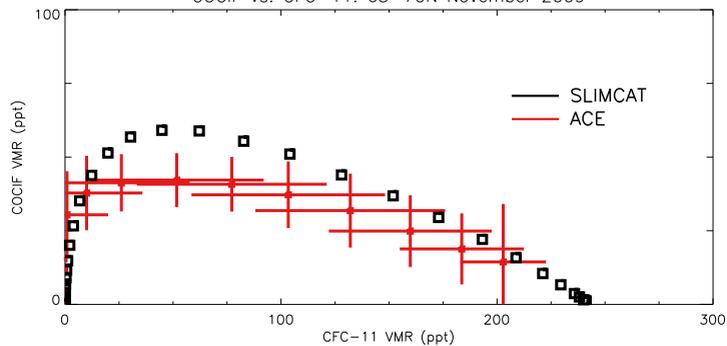
COCIF vs. CFC-11: 65-70S January 2010
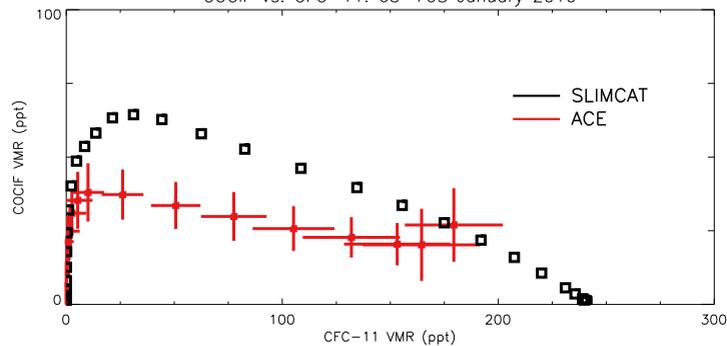
COCIF vs. CFC-11: 65-70S May 2010
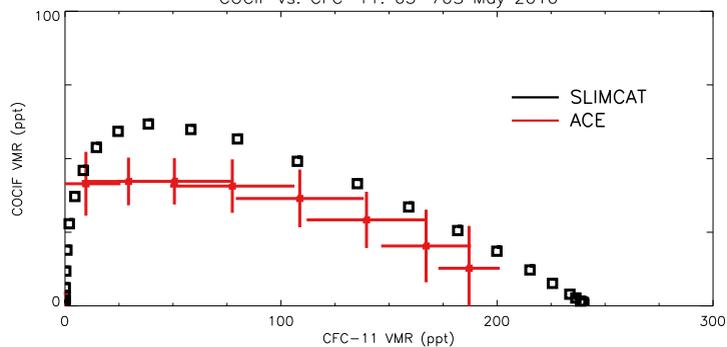
COCIF vs. CFC-11: 65-70N July 2010
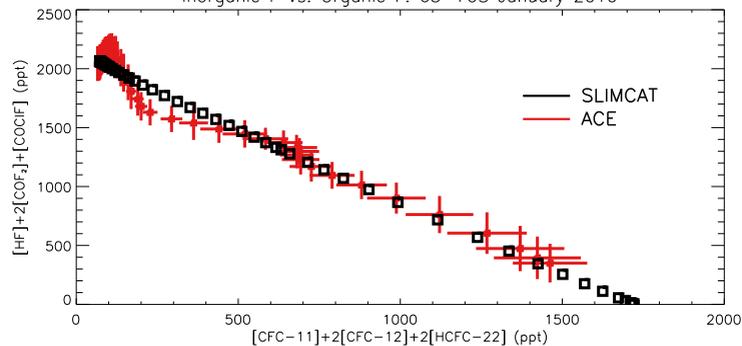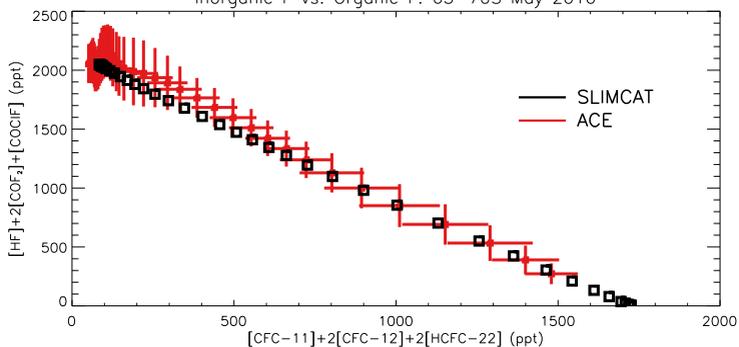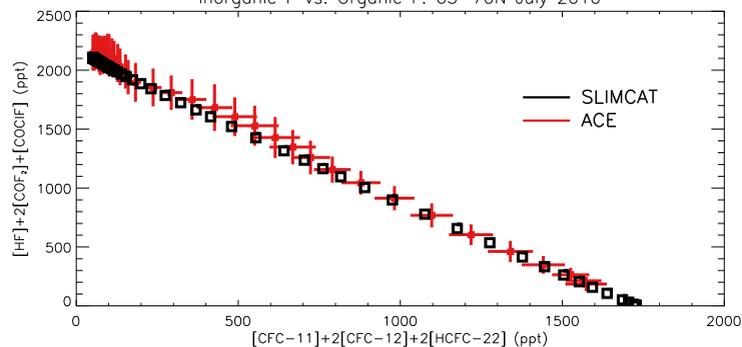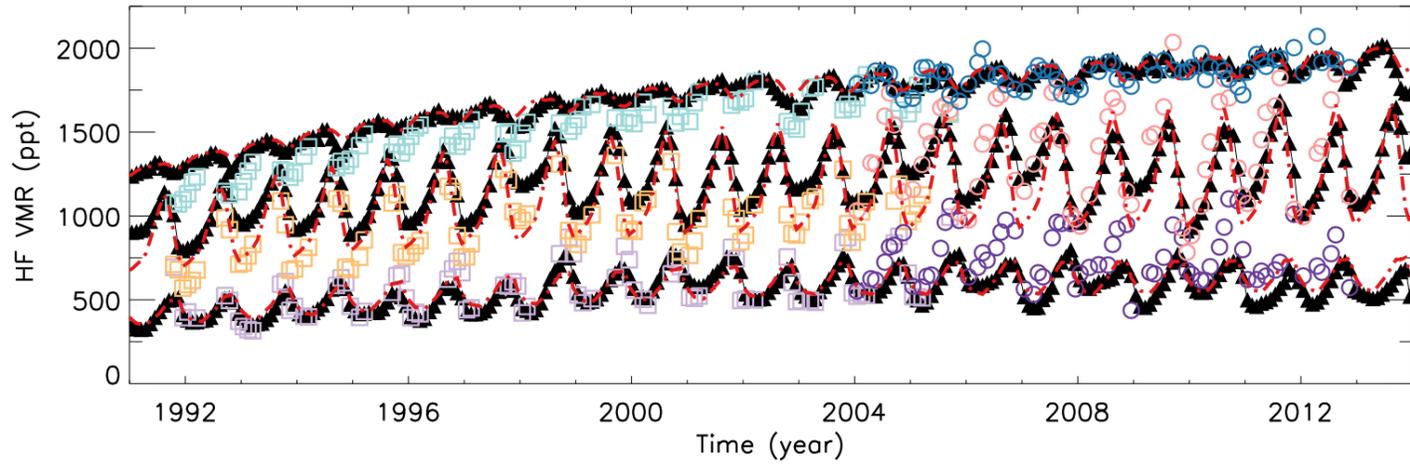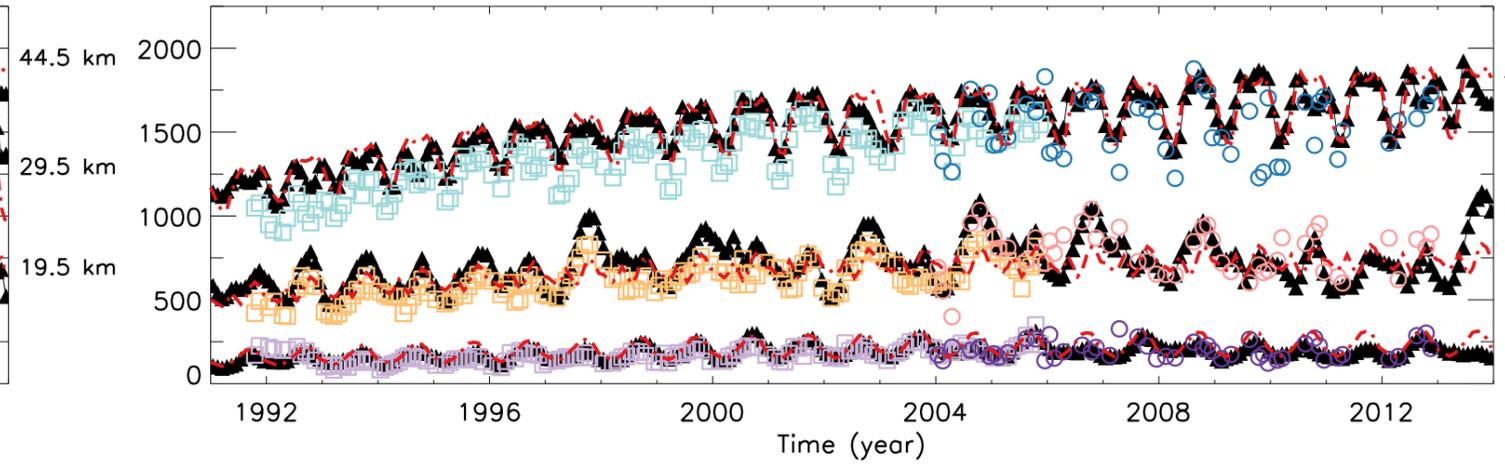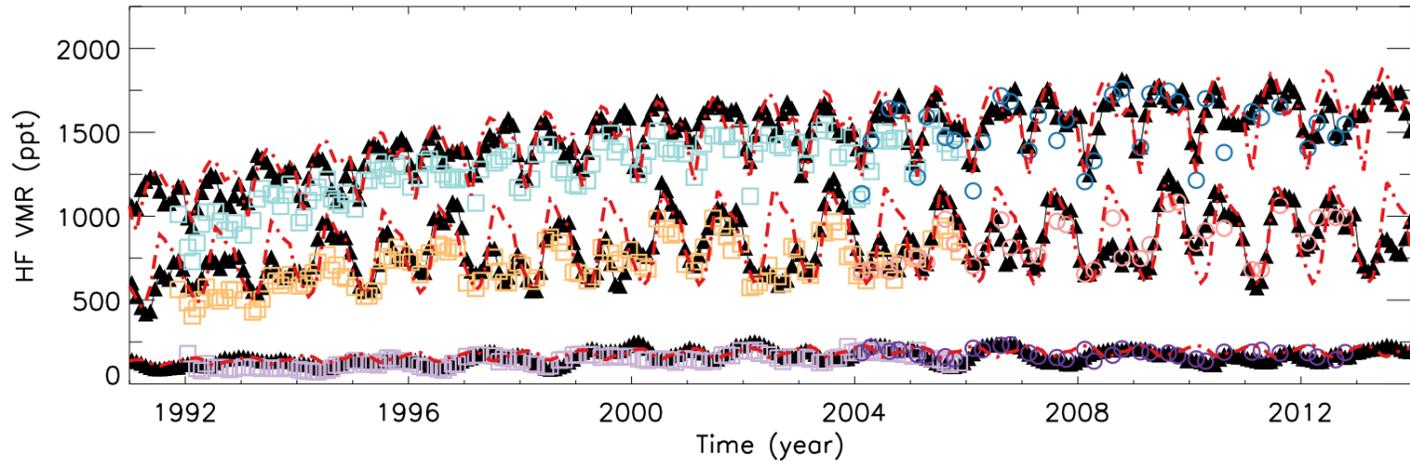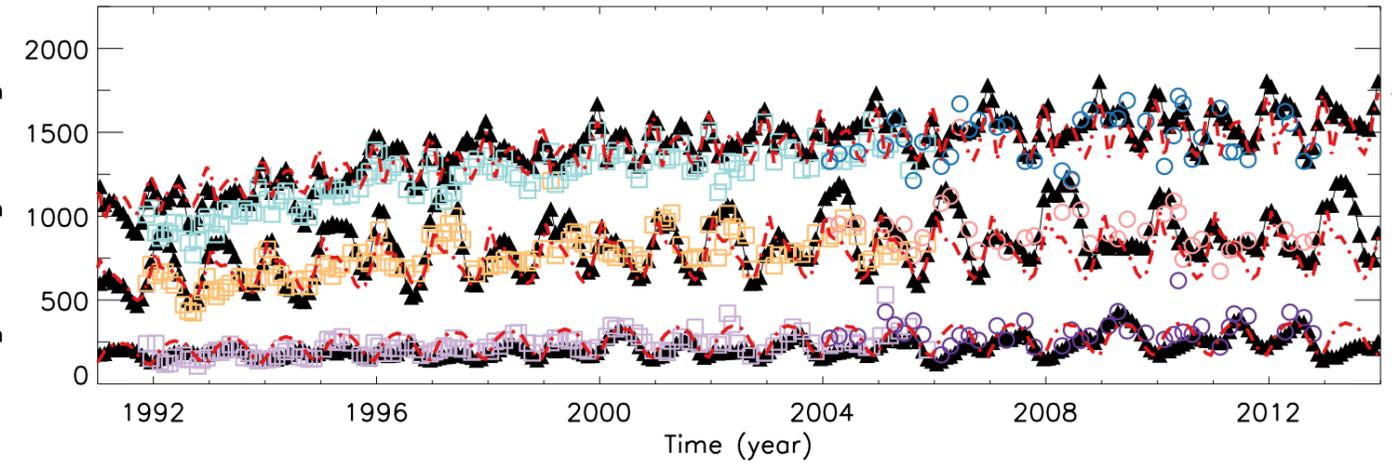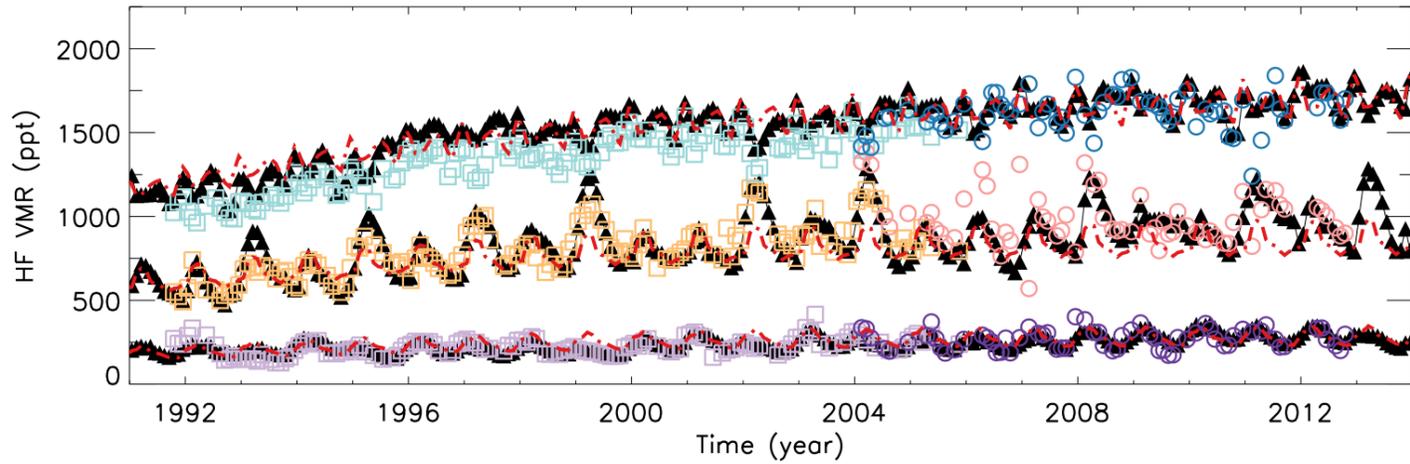
Latitude: −70° to −60°   Latitude: −30° to −20°   Latitude: −10° to 0°   Latitude: 10° to 20°   Latitude: 30° to 40°   Latitude: 60° to 70°
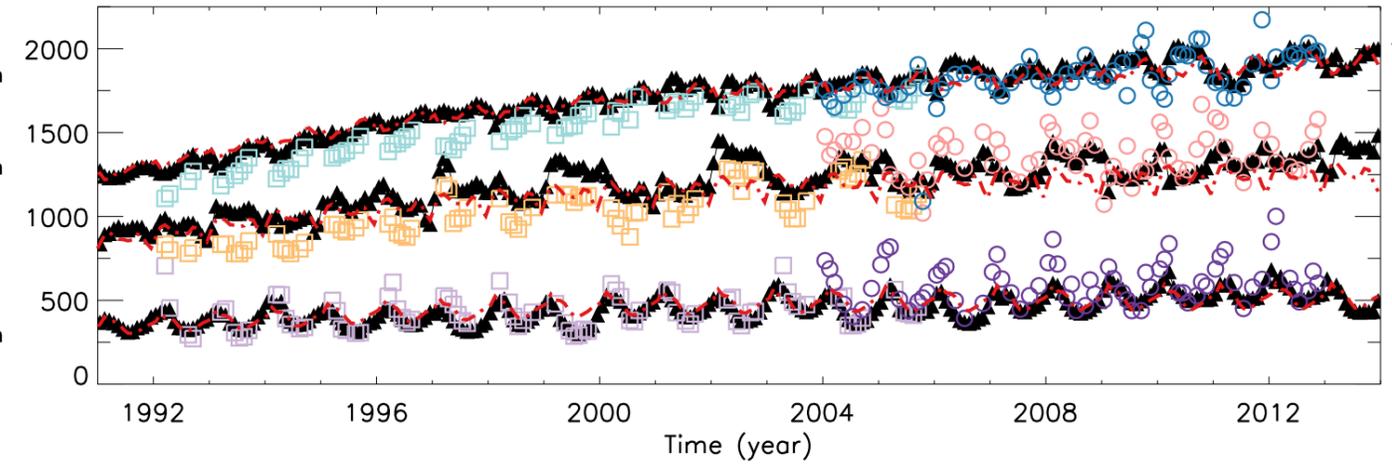
□ HALOE   ○ ACE   ▲ SLIMCAT   SLIMCAT (fixed)
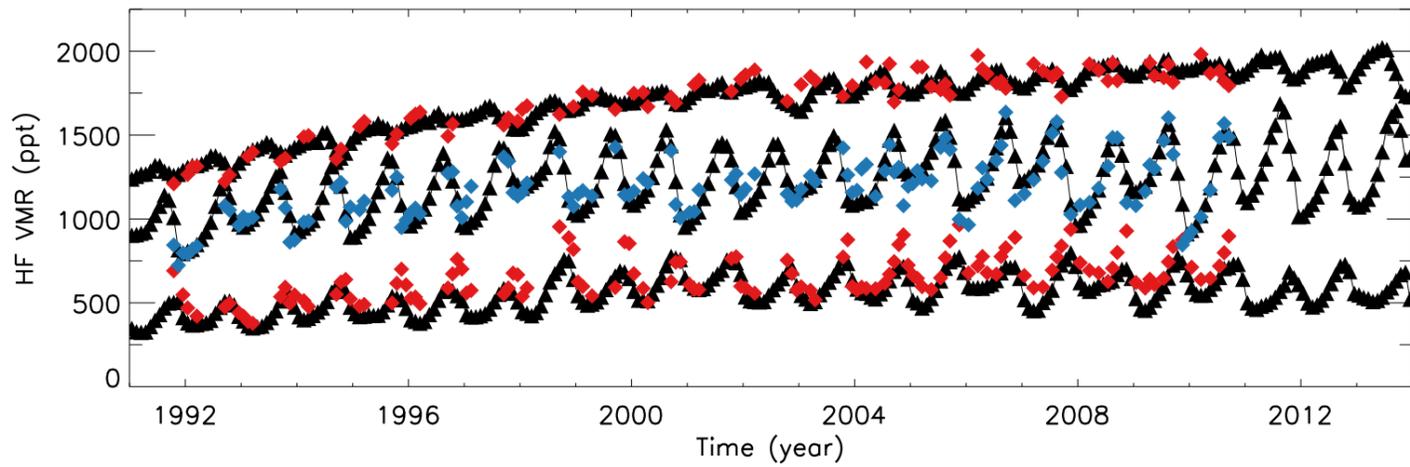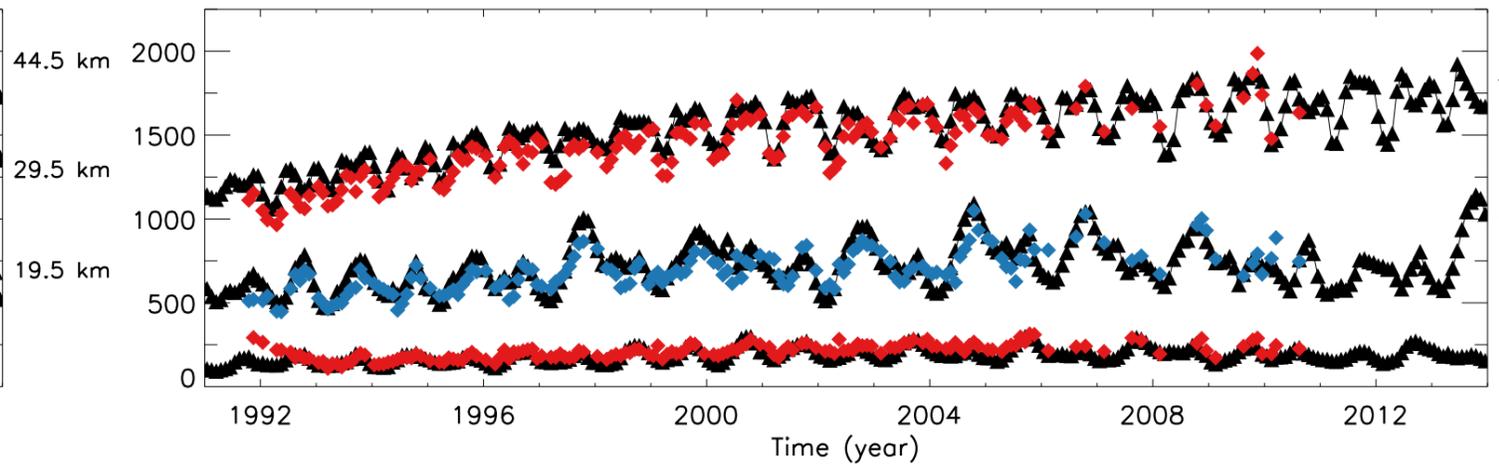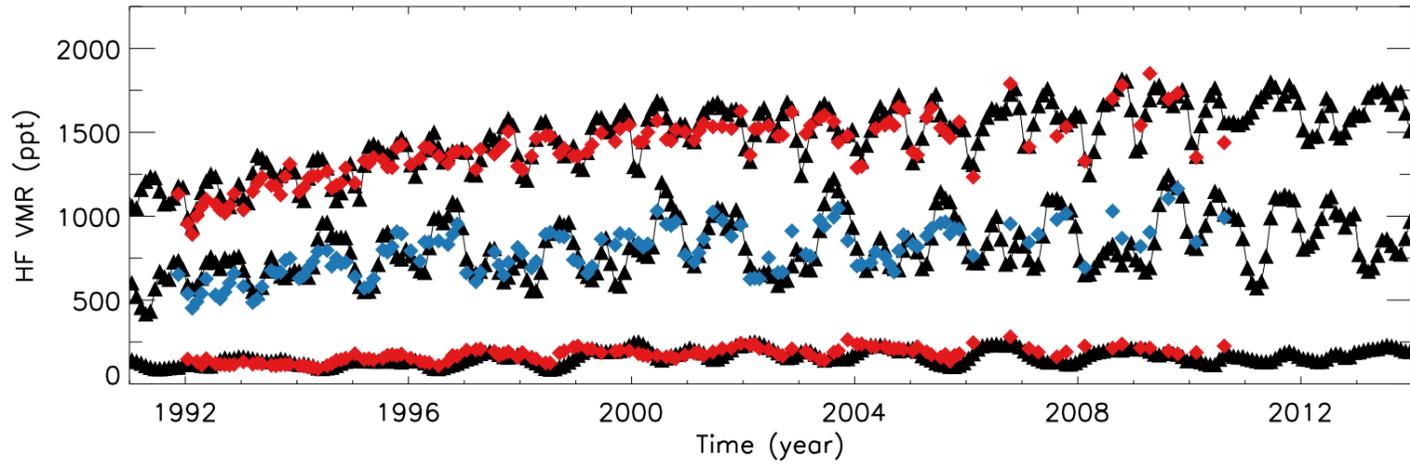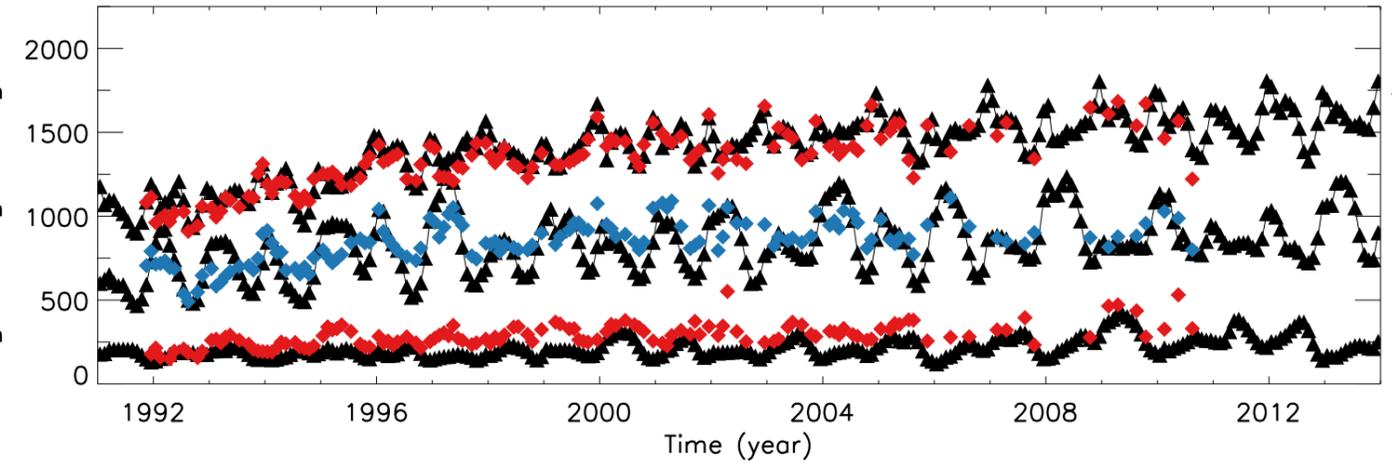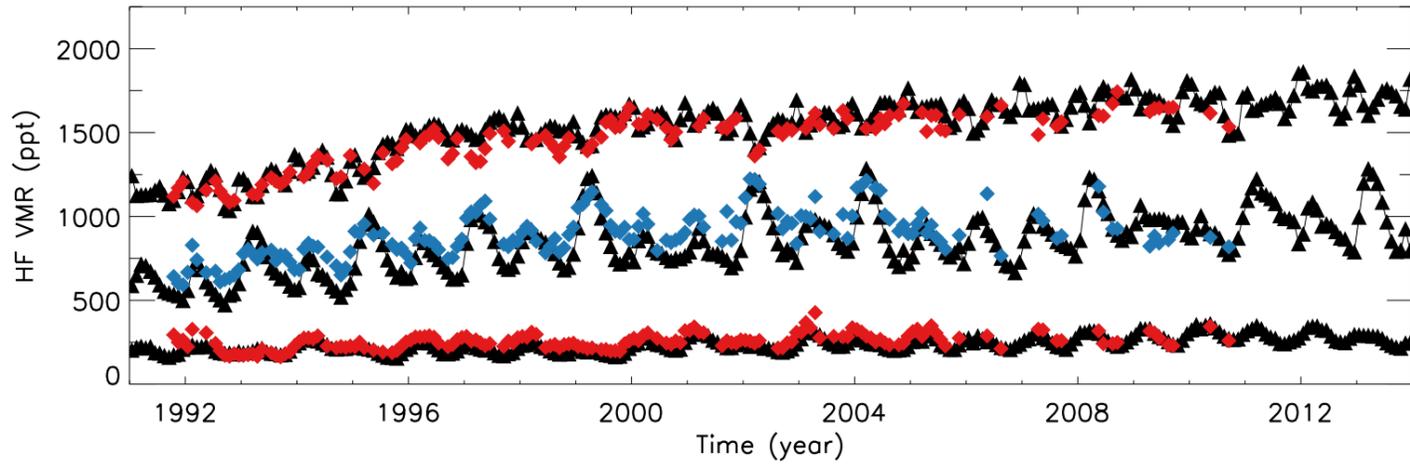
Latitude: −70° to −60° Latitude: −30° to −20° Latitude: −10° to 0° Latitude: 10° to 20° Latitude: 30° to 40° Latitude: 60° to 70°
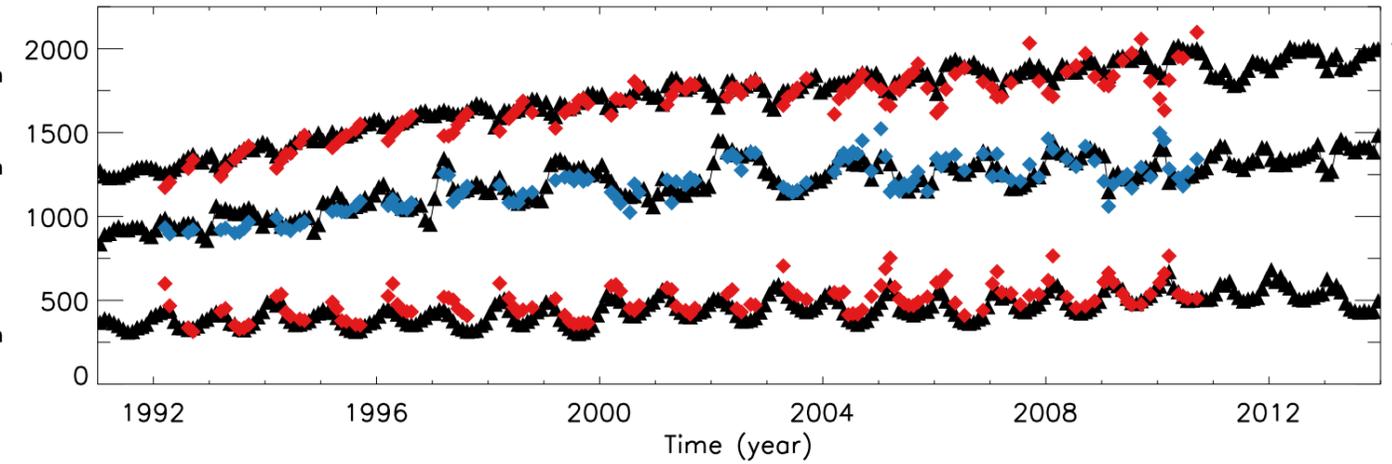
◆ GOZCARDS   ▲ SLIMCAT

ACE HF trends (January 2004 to December 2012)
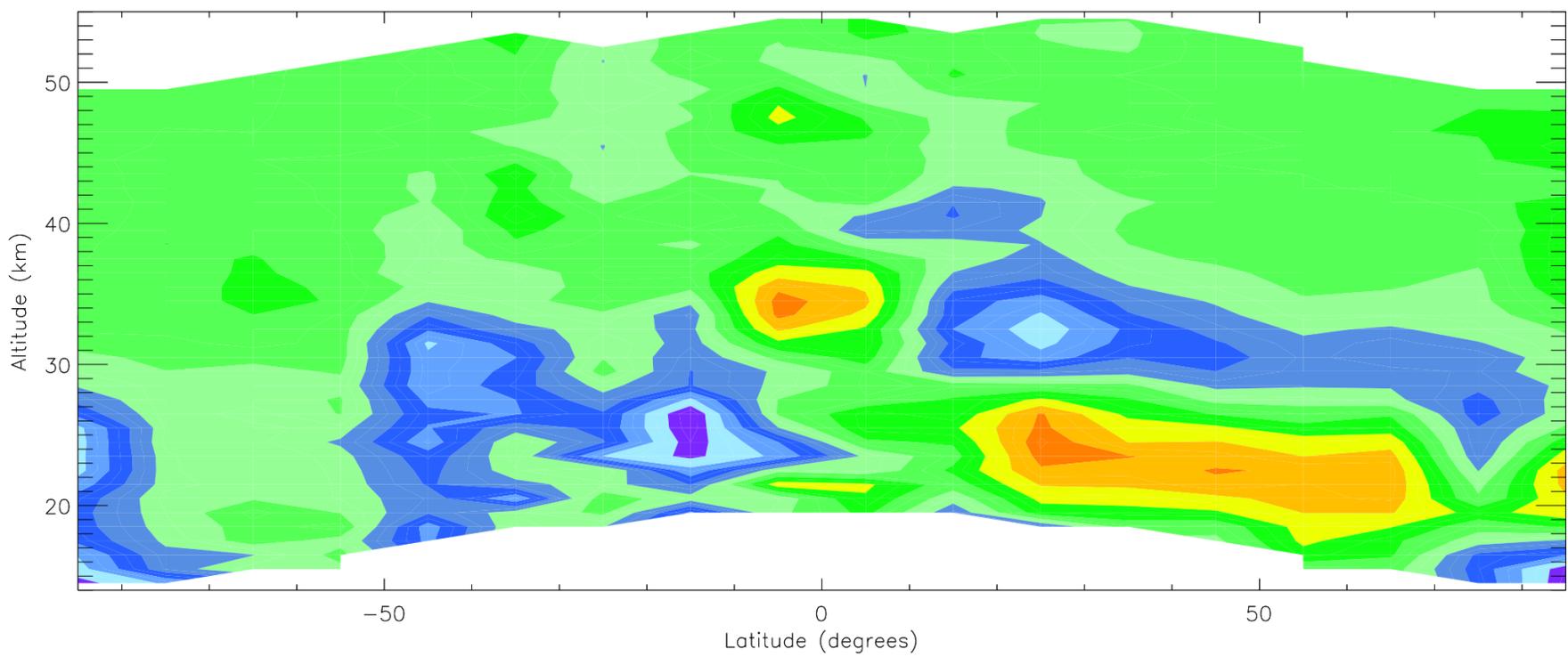
SLIMCAT HF trends (January 2004 to December 2012)
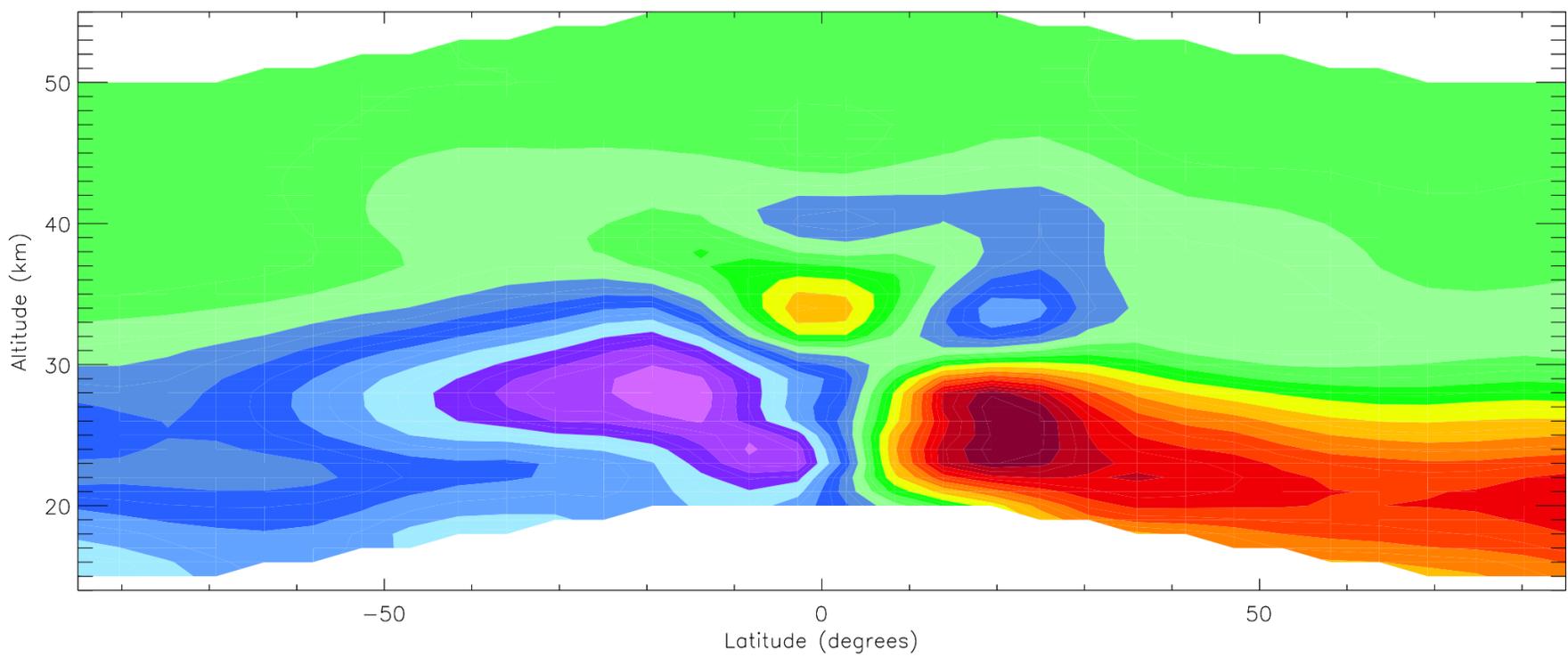
SLIMCAT HF trends (January 2004 to December 2012) − fixed to 2000 dynamics
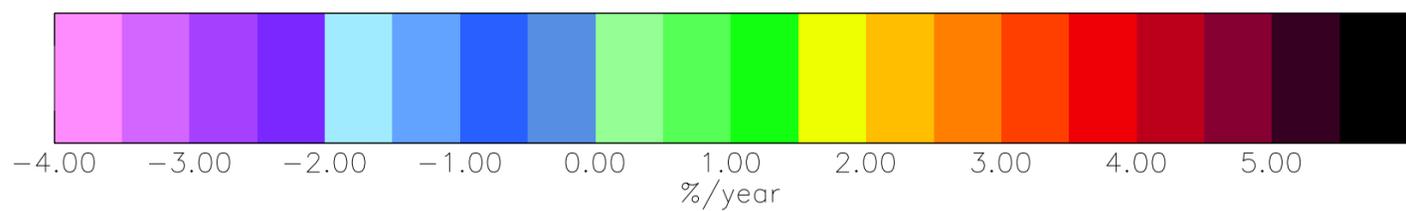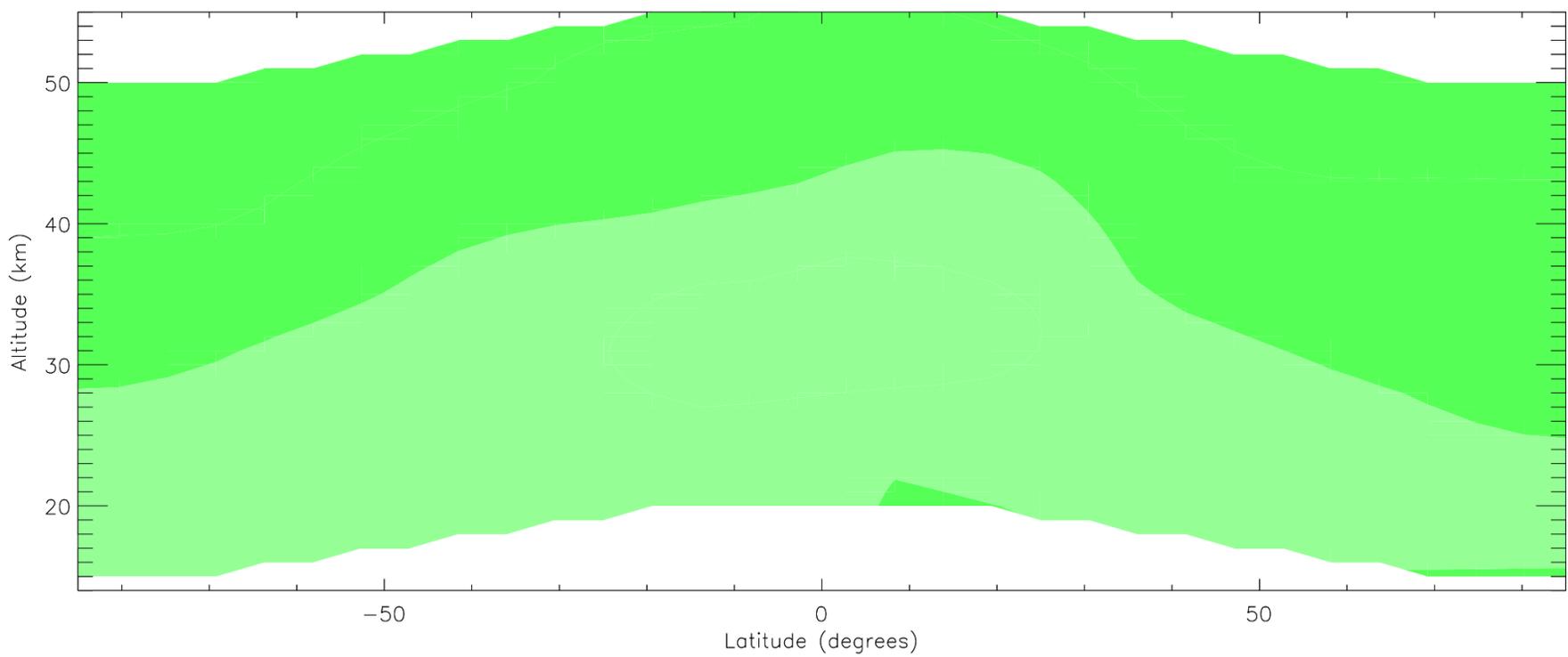
%/year

HALOE HF trends (January 1991 to December 1997)

SLIMCAT HF trends (January 1991 to December 1997)

SLIMCAT HF trends (January 1991 to December 1997) – fixed to 2000 dynamics
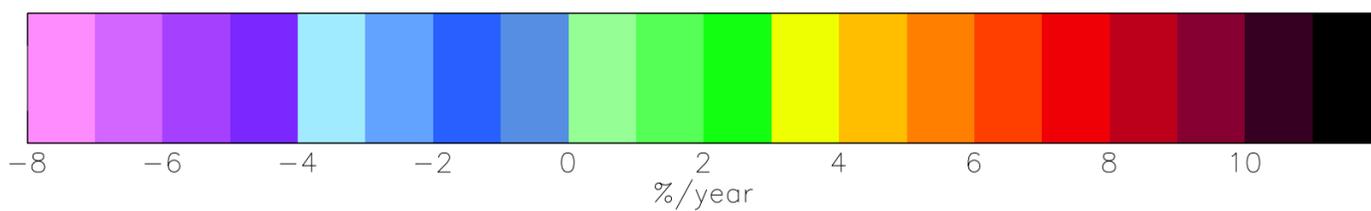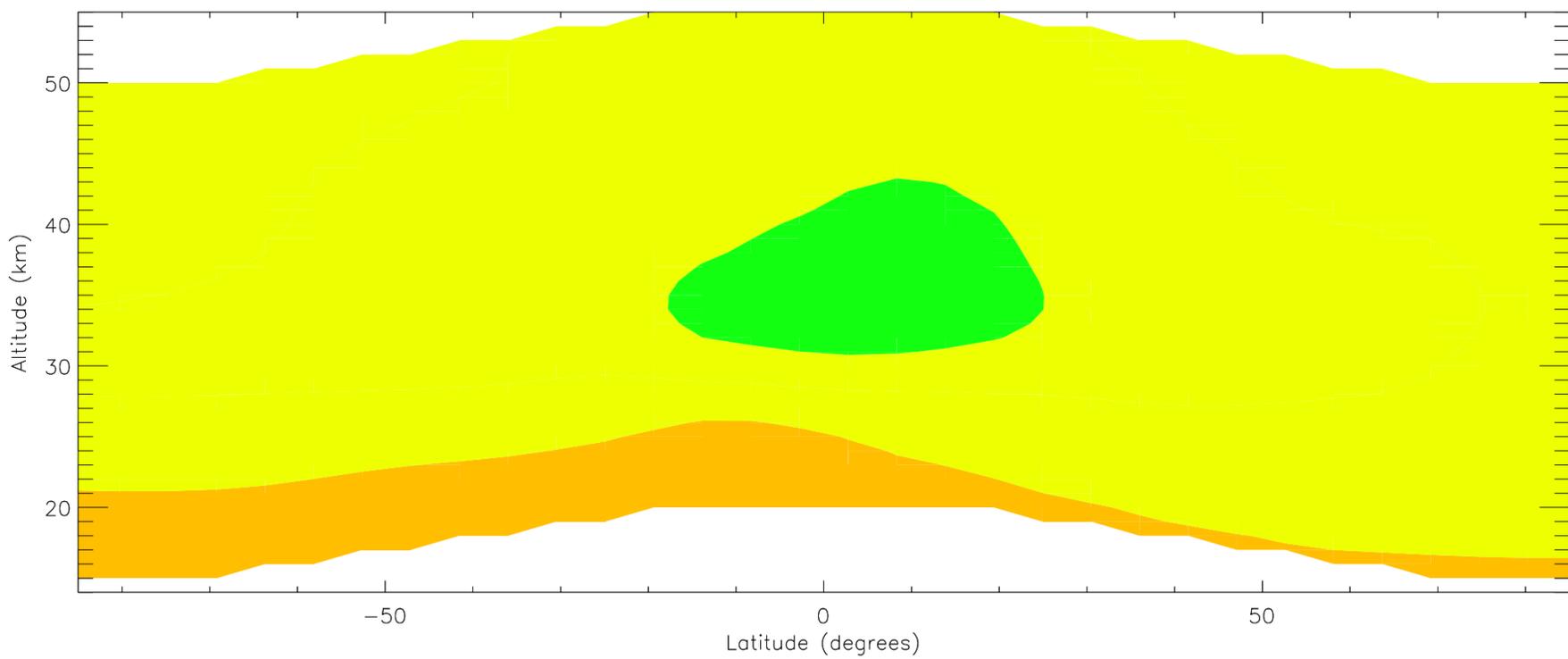
HALOE HF trends (January 1998 to November 2005)
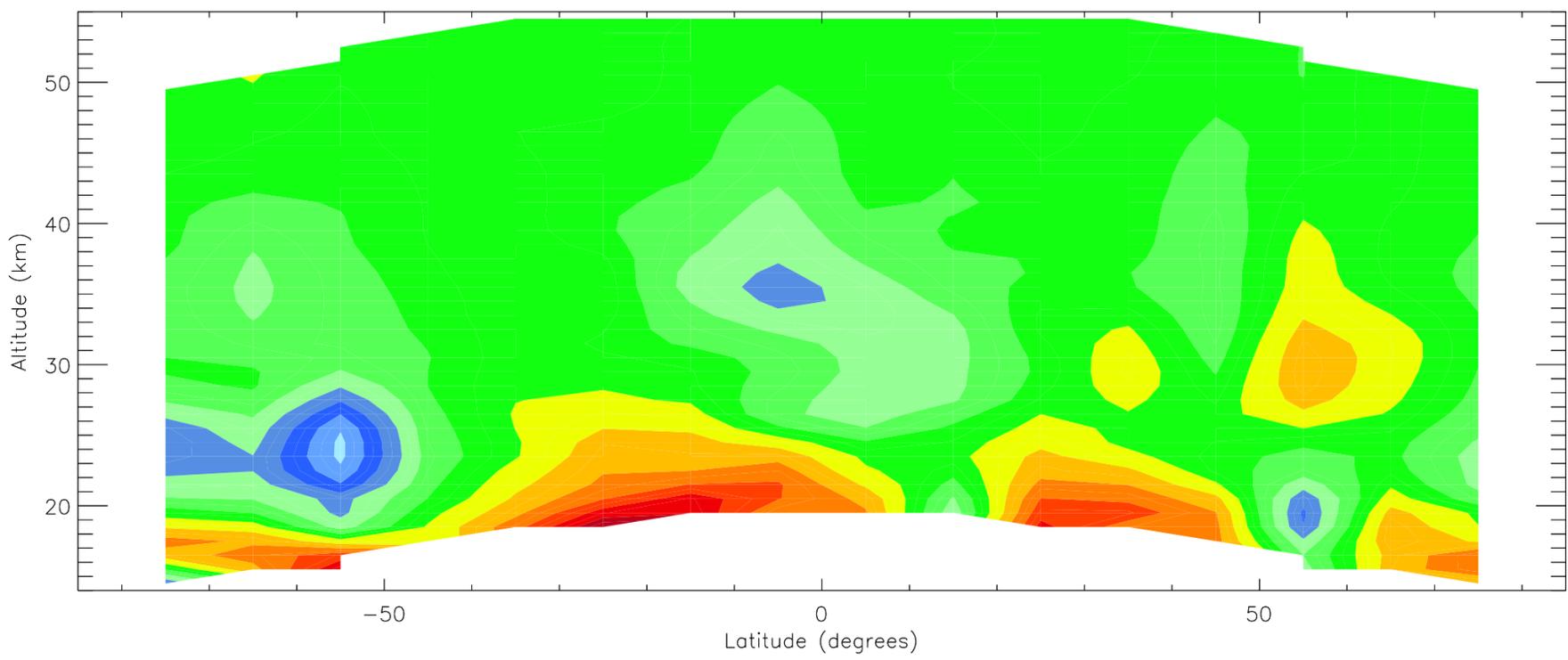
SLIMCAT HF trends (January 1998 to November 2005)
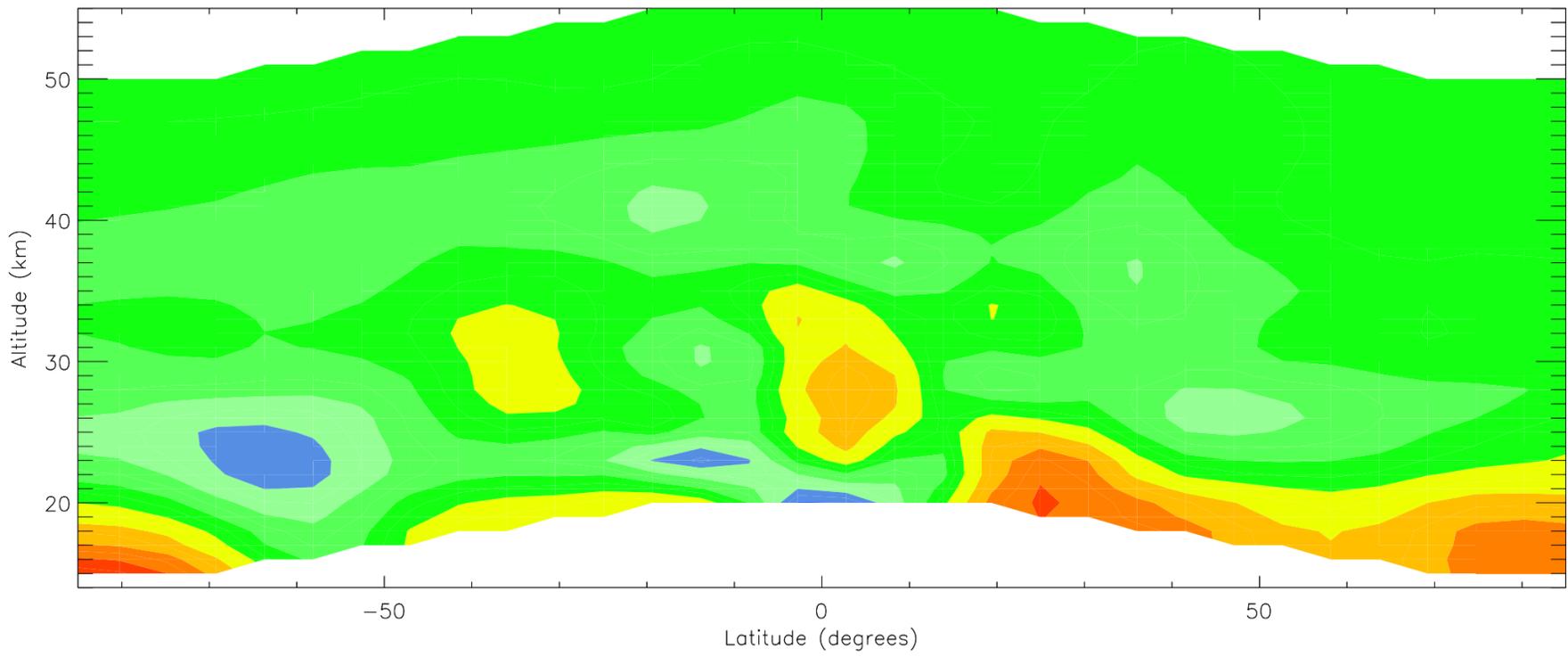
SLIMCAT HF trends (January 1998 to November 2005) – fixed to 2000 dynamics

%/year